The schizophrenia susceptibility factor dysbindin and its associated complex sort cargoes from cell bodies to the synapse

Jennifer Larimore[a], Karine Tornieri[a], Pearl V. Ryder[a,b], Avanti Gokhale[a], Stephanie A. Zlatic[a,b], Branch Craige[a,b,*], Joshua D. Lee[c], Konrad Talbot[c], Jean-Francois Pare[d], Yoland Smith[d], and Victor Faundez[a,b,e]

[a]Department of Cell Biology, [b]Graduate Program in Biochemistry, Cell, and Developmental Biology, Emory University, Atlanta, GA 30322; [c]Center for Neurobiology and Behavior, Department of Psychiatry, University of Pennsylvania, Philadelphia, PA 19104; [d]Department of Neurology and Yerkes National Primate Research Center, [e]Center for Neurodegenerative Disease, Emory University, Atlanta, GA 30322

ABSTRACT **Dysbindin assembles into the biogenesis of lysosome-related organelles complex 1 (BLOC-1), which interacts with the adaptor protein complex 3 (AP-3), mediating a common endosome-trafficking route. Deficiencies in AP-3 and BLOC-1 affect synaptic vesicle composition. However, whether AP-3-BLOC-1–dependent sorting events that control synapse membrane protein content take place in cell bodies upstream of nerve terminals remains unknown. We tested this hypothesis by analyzing the targeting of phosphatidylinositol-4-kinase type II α (PI4KIIα), a membrane protein present in presynaptic and postsynaptic compartments. PI4KIIα copurified with BLOC-1 and AP-3 in neuronal cells. These interactions translated into a decreased PI4KIIα content in the dentate gyrus of dysbindin-null BLOC-1 deficiency and AP-3–null mice. Reduction of PI4KIIα in the dentate reflects a failure to traffic from the cell body. PI4KIIα was targeted to processes in wild-type primary cultured cortical neurons and PC12 cells but failed to reach neurites in cells lacking either AP-3 or BLOC-1. Similarly, disruption of an AP-3–sorting motif in PI4KIIα impaired its sorting into processes of PC12 and primary cultured cortical neuronal cells. Our findings indicate a novel vesicle transport mechanism requiring BLOC-1 and AP-3 complexes for cargo sorting from neuronal cell bodies to neurites and nerve terminals.**

Monitoring Editor
Keith E. Mostov
University of California, San Francisco

Received: Jul 5, 2011
Revised: Sep 8, 2011
Accepted: Oct 7, 2011

INTRODUCTION

Cell polarity is established and maintained, in part, by selective targeting of membrane components to distinct organelles or plasma membrane domains. This is particularly evident in neurons, where membrane components transported in vesicular carriers generated in the cell body are selectively targeted to distal compartments of axons or dendrites. Alternatively, vesicle carriers are generated locally at synaptic domains. Vesicular carriers are generated by cytosolic coats, which specify their protein and lipid composition (Bonifacino and Glick, 2004). Diverse coats and accessory proteins generate a multitude of vesicles in eukaryotic cells (Robinson, 2004). Although the diversity of vesicle carriers and their pathways have been intensely studied in yeast and mammalian fibroblastoid cell lines, knowledge about the diversity and specializations of vesicle transport pathways in polarized cells is limited. Clathrin and clathrin-binding adaptors orchestrate vesicle biogenesis, and in polarized cells they contribute to specialized transport mechanisms (Folsch *et al.*, 1999, 2003; Deborde *et al.*, 2008). For example, heterotetrameric clathrin adaptors AP-1–4 participate in the biogenesis of synaptic vesicles at the nerve terminal (Voglmaier *et al.*, 2006; Glyvuk *et al.*, 2010; Haucke *et al.*,

This article was published online ahead of print in MBoC in Press (http://www.molbiolcell.org/cgi/doi/10.1091/mbc.E11-07-0592) on October 12, 2011.

*Present address: Department of Cell Biology, University of Massachusetts Medical School, Worcester, MA 01655.

Address correspondence to: Victor Faundez (vfaunde@emory.edu).

Abbreviations used: AP-3, Adaptor Protein Complex 3; BLOC-1, biogenesis of lysosome-related organelles complex 1; DSP, dithiobissuccinimidyl propionate; EGFP, enhanced green fluorescent protein; FBS, fetal bovine serum; FRAP fluorescence recovery after photobleaching; Ig, immunoglobulin; mAb, monoclonal antibody; PBS, phosphate-buffered saline; PI4KIIα, phosphatidylinositol-4-kinase type IIα; VAMP2, vesicle-associated membrane protein 2; VAMP7, vesicle-associated membrane protein 7.

2011), delivery of receptors to dendrites (Dwyer *et al.*, 2001; Matsuda and Yuzaki, 2009), binding of synaptic vesicle membrane proteins (Horikawa *et al.*, 2002), processing of the amyloid precursor protein (Burgos *et al.*, 2010), and trafficking to autophagosomes in axons (Matsuda *et al.*, 2008). Human mutations in clathrin adaptor isoforms trigger neuropathology ranging from cerebral palsy to mental retardation, emphasizing central roles played by adaptor complexes in neuronal homeostasis (Tarpey *et al.*, 2006; Saillour *et al.*, 2007; Borck *et al.*, 2008; Montpetit *et al.*, 2008; Moreno-De-Luca *et al.*, 2011). Vesicle carriers from the cell body must deliver membrane proteins that will later recycle locally in presynaptic or postsynaptic compartments. It is surprising that the diversity of cell body–derived vesicle carriers bound to synapses, the coat-adaptor mechanisms that assemble these vesicles, and their contents remain largely unexplored (Lasiecka and Winckler, 2011; Winckler and Choo Yap, 2011).

Defects in vesicle-trafficking mechanisms may also promote pathogenesis of major psychoses, including schizophrenia (Ryder and Faundez, 2009; Karayiorgou *et al.*, 2010). Genome-wide analyses reveal strong associations between genes encoding adaptor-binding proteins and schizophrenia (Ryder and Faundez, 2009). Of particular interest is dysbindin, the product encoded by the *DTNBP1* locus. *DTNBP1* ranks high among all genes studied thus far in terms of their strength of association with schizophrenia risk. Of importance, dysbindin protein levels are reduced in the prefrontal cortex, superior temporal gyrus, and hippocampal formation (hippocampus plus dentate gyrus) of schizophrenia patients, further underscoring the association between dysbindin function and schizophrenia pathogenesis (Talbot *et al.*, 2004, 2011; Tang *et al.*, 2009a). However, *DTNBP1* genetic association with disease is not universal among all human populations (Ross *et al.*, 2006; Allen *et al.*, 2008; Sun *et al.*, 2008; Talbot *et al.*, 2009; Ghiani and Dell'Angelica, 2011; Mullin *et al.*, 2011).

Dysbindin is a subunit of the octameric biogenesis of lysosome-related organelles complex 1 (BLOC-1 complex; Li *et al.*, 2003; Starcevic and Dell'Angelica, 2004; Di Pietro and Dell'Angelica, 2005). The BLOC-1 complex is assembled by dysbindin, pallidin, muted, snapin, cappuccino, and BLOS1-3 subunits (Li *et al.*, 2004; Di Pietro and Dell'Angelica, 2005; Wei, 2006; Raposo and Marks, 2007; Dell'Angelica, 2009). The BLOC-1 complex binds to the clathrin adaptor protein complex AP-3 (Di Pietro *et al.*, 2006; Newell-Litwa *et al.*, 2010), a heterotetramer constituted of δ, β3, μ3, and σ3 subunits. The genes encoding the component proteins in AP-3 and BLOC-1 belong to a group of 15 genetic loci in mice. Mutations in some of these loci trigger Hermansky–Pudlak syndrome in humans, which is characterized by, but not limited to, pigment dilution, bleeding diathesis, and pulmonary fibrosis—phenotypes that are recapitulated in mouse models of this syndrome. These mutated genes encode products that belong to five distinct cytosolic complexes: AP-3, BLOC-1, BLOC-2, BLOC-3, and the HOPS complex (Li *et al.*, 2004; Di Pietro and Dell'Angelica, 2005; Wei, 2006; Raposo and Marks, 2007; Dell'Angelica, 2009). At the cellular level, AP-3 and BLOC-1 subunits localize to nerve terminals and/or axons, and deficiencies in these complexes alter the composition of synaptic vesicles and the surface expression of neurotransmitter receptors (Talbot *et al.*, 2006; Iizuka *et al.*, 2007; Ji *et al.*, 2009; Newell-Litwa *et al.*, 2009, 2010; Tang *et al.*, 2009b; Marley and von Zastrow, 2010). These cellular defects trigger neurobehavioral phenotypes from *Drosophila* to mouse, some of which resemble those found in schizophrenia patients (Hattori *et al.*, 2008; Bhardwaj *et al.*, 2009; Cox *et al.*, 2009; Dickman and Davis, 2009; Talbot, 2009; Cheli *et al.*, 2010; Papaleo *et al.*, 2010). These observations highlight fundamental vesicle transport pathways controlled by BLOC-1 and AP-3 in neurons. However, a central question not yet addressed is whether BLOC-1 and AP-3 perform sorting functions uniquely restricted to the synapse (Voglmaier *et al.*, 2006) and/or whether these complexes assemble vesicle carriers in cell bodies destined to deliver membrane proteins that are later incorporated into synapses.

Here we explore polarized neuronal membrane-trafficking routes requiring BLOC-1 and AP-3, using the membrane-anchored lipid kinase phosphatidylinositol-4-kinase type IIα (PI4KIIα) as a reporter. Our focus on PI4KIIα is based on its capacity to bind the AP-3 complexes and to regulate AP-3 recruitment to membranes (Craige *et al.*, 2008; Salazar *et al.*, 2009). We demonstrate that PI4KIIα copurifies with BLOC-1 complexes assembled with either tagged dysbindin or muted subunits, as well as with AP-3. These biochemical interactions were confirmed genetically, since a PI4KIIα synaptic depletion phenotype in the dentate gyrus of dysbindin-null *sandy* mice was phenocopied in that area of the brains of AP-3-null *mocha* mice and in mice lacking the muted or pallidin components of BLOC-1. PI4KIIα synaptic depletion suggested that BLOC-1 and AP-3 regulate delivery of membrane proteins from cell bodies to nerve terminals. Consistent with this hypothesis, analysis of the subcellular localization of wild-type PI4KIIα or a mutant form unable to bind AP-3 and BLOC-1 indicated that the interaction of PI4KIIα with AP-3-BLOC-1 was required for PI4KIIα export from cell bodies to neurites. Similarly, wild-type PI4KIIα failed to reach neurites in neurons of AP-3– or BLOC-1–mutant mice. Our findings reveal a novel vesicle transport mechanism in which BLOC-1, in association with the AP-3 complex, delivers specific cargoes from neuronal cell bodies to neurites and nerve terminals. We propose that defects in the dysbindin/BLOC-1 vesicle-trafficking pathway and the resulting mislocalization of specific cargo molecules contribute to the pathogenesis of complex psychiatric disorders.

RESULTS

Phosphatidylinositol-4-kinase type IIα biochemically and genetically interacts with BLOC-1 and AP-3

We previously showed that PI4KIIα binding to AP-3 is sensitive to the dose of the dysbindin-containing BLOC-1 complex (Salazar *et al.*, 2009). Precipitation of AP-3 complexes with AP-3 δ antibodies specifically coprecipitated PI4KIIα from wild-type fibroblasts (Figure 1A, compare lanes 3 and 5). In contrast, the association of PI4KIIα to AP-3 complexes was decreased in BLOC-1–null cells carrying the *Pldn*$^{pa/pa}$ allele (Figure 1A, compare lanes 5 and 6). Thus we tested the hypothesis that dysbindin associates with the adaptor complex AP-3 and PI4KIIα, in addition to its interactions within the BLOC-1 complex. We expressed N-terminal FLAG-tagged dysbindin in SH-SY5Y neuroblastoma cells. Protein complexes coprecipitating with FLAG-dysbindin were isolated from cells treated in the absence or presence of dithiobis(succinimidyl proprionate) (DSP; Figure 1). DSP is a cell-permeable and reducible cross-linker used here to stabilize protein–protein interactions labile to stringent purification (Lomant and Fairbanks, 1976; Salazar *et al.*, 2009; Zlatic *et al.*, 2010). Isolation of FLAG-dysbindin protein complexes with FLAG antibodies coprecipitated the BLOC-1 subunits muted and pallidin (Figure 1B, lane 7), as well as the AP-3 subunits δ, β3, and σ3 (Figure 1B, lane 8). Dysbindin's associations with AP-3 subunits required stabilization with DSP (Figure 1B, lane 8). These associations with FLAG-dysbindin beads were specific, as determined by their absence from beads alone (Figure 1B, lanes 3 and 4), beads coated with control SV2 antibody (Figure 1B, lanes 5 and 6), and competition with an excess FLAG antigenic peptide during bead incubation

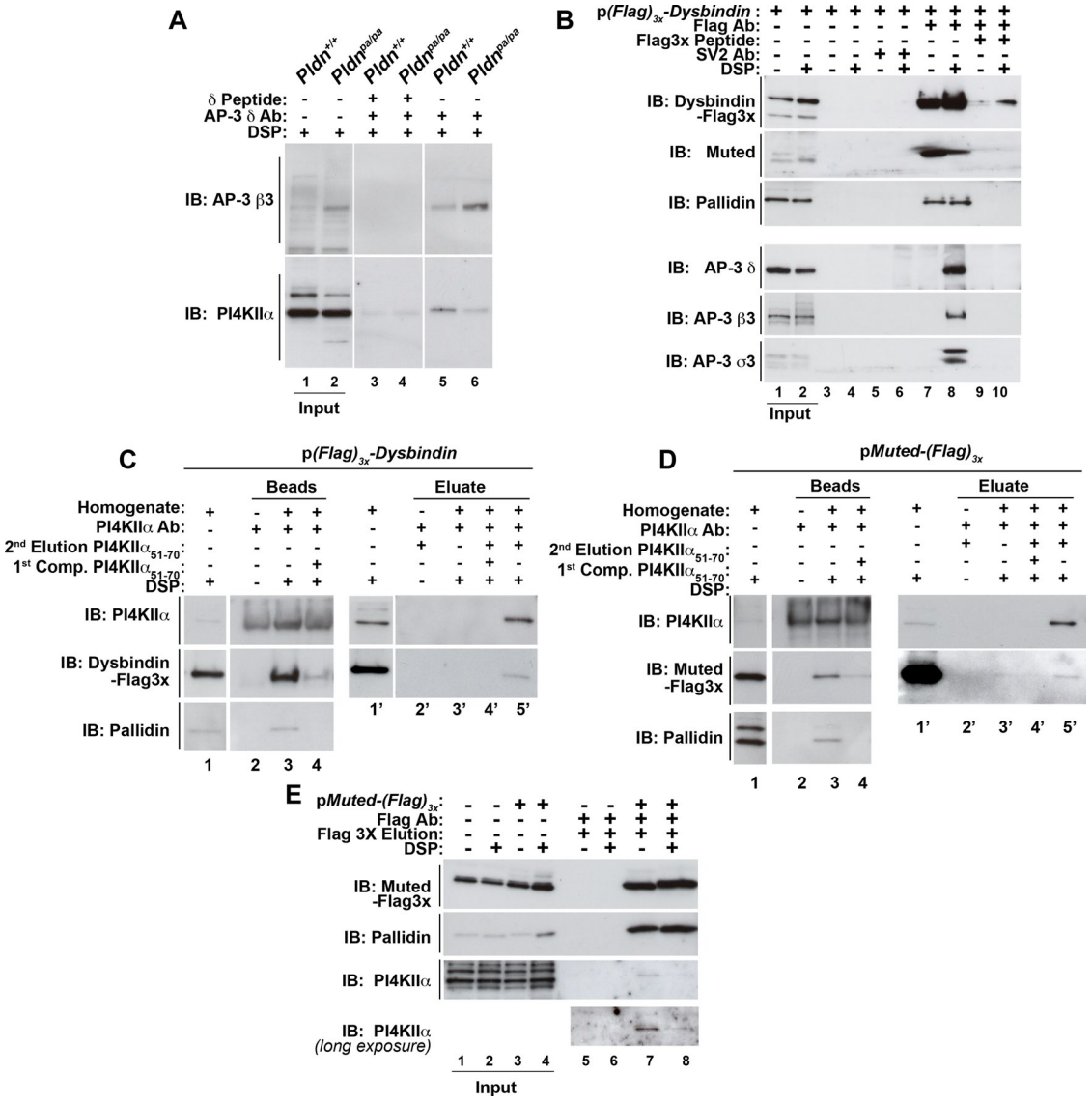

FIGURE 1: Dysbindin coprecipitates BLOC-1 subunits, AP-3 complexes, and PI4KIIα. (A) Wild-type (*Pldn*$^{+/+}$, odd lanes) or pallidin-deficient (*Pldn*$^{pa/pa}$, even lanes) mouse skin primary culture fibroblasts were treated with DSP, detergent solubilized, and extracts precipitated with magnetic beads with antibodies against AP-3 delta (lanes 3–6) in either the absence (lanes 5 and 6) or presence (lanes 3 and 4) of delta antigenic peptide as an immunoprecipitation control. (B) SH-SY5Y stably expressing triple FLAG dysbindin treated in the absence or presence of DSP were solubilized in detergent and extracts precipitated with magnetic beads alone as controls (lanes 3–6), with antibodies against FLAG tag (lanes 7–10). Precipitations were performed in the absence or presence of an excess of FLAG peptide (lanes 9 and 10). An irrelevant antibody (SV2, lanes 5 and 6) was used to confirm specificity. (C) SH-SY5Y FLAG dysbindin or (D) SH-SY5Y FLAG muted cell extracts were precipitated with PI4KIIα antibodies (lanes 3, 4, and 3′–5′) in either the absence or presence of PI4KIIα peptide 51-70 to outcompete binding of PI4KIIα complexes to beads (first Competition [Comp.], lanes 4 and 4′). Protein complexes bound to beads were eluted with SDS–PAGE sample buffer (lanes 2–4). The band detected in PI4KIIα blots in lanes 1 and 4 corresponds to the rabbit anti-PI4KIIα immunoglobulin G also used for immunoprecipitation. Alternatively, PI4KIIα protein complexes were eluted from beads with buffer in either the absence (lane 3′) or presence of 200 μM PI4KIIα peptide 51-70 (second elusion, lane 5′). (E) Untransfected SH-SY5Y (lanes 1, 2, 5, and 6) or SH-SY5Y FLAG muted cells treated in the absence or presence of DSP were solubilized in detergent and extracts were precipitated with FLAG antibodies (lanes 5–8), and FLAG muted protein complexes were eluted from beads with 200 μM FLAG peptide (lanes 5–8). Note that PI4KIIα coprecipitates with FLAG-tagged muted even in the absence of DSP (lane 7). Specificity was determined by using cell extracts from nontransfected cells (lanes 5 and 6). Immune complexes resolved by SDS–PAGE were analyzed by immunoblot with antibodies against FLAG, the BLOC-1 subunits pallidin and muted, AP-3 subunits (δ, β3, σ3), and PI4KIIα. Inputs are 10%, and in B–D inputs are lanes 1 and 1′.

with cell extracts (Figure 1B, lanes 9 and 10). We next tested whether endogenous PI4KIIα copurified with BLOC-1 subunits by PI4KIIα immunoaffinity chromatography. PI4KIIα was isolated with an antibody directed against amino acids 51–70 from human PI4KIIα, and PI4KIIα protein complexes were selectively eluted with the PI4KIIα peptide 51–70 used to generate the PI4KIIα antibody (Supplemental

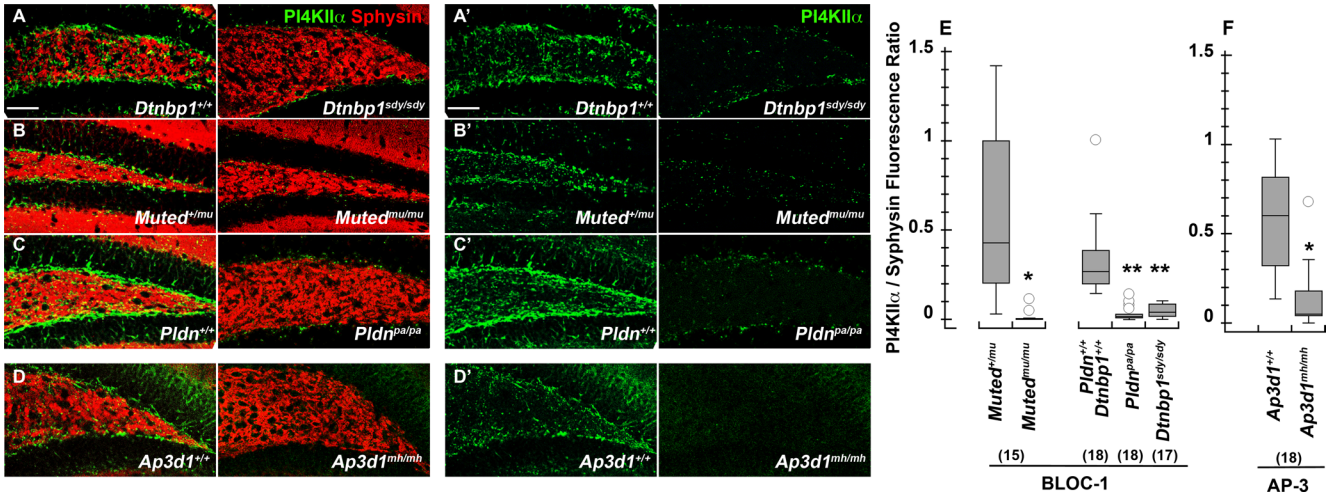

FIGURE 2: Dentate gyrus PI4KIIα content is reduced in the neuropil of BLOC-1– and AP-3–deficient mice. The dentate gyrus of the hippocampal formation from 6- to 8-wk-old control (A–D), BLOC-1–deficient *sandy* (*Dtnbp1*$^{sdy/sdy}$), *muted* (*Muted*$^{mu/mu}$), and *pallid* (*Pldn*$^{pa/pa}$) and AP-3–deficient *mocha* (*Ap3d1*$^{mh/mh}$) mice was stained with antibodies against PI4KIIα (green) and the synaptic vesicle marker synaptophysin (red). (E) Total pixels for synaptophysin and PI4KIIα were quantified by MetaMorph analysis and expressed as a ratio of PI4KIIα to synaptophysin pixel counts. Numbers in parentheses represent the number of independent sections stained from three animals. *$p < 0.0001$; **$p < 0.005$. Bar, 50 μm.

Figure S1). PI4KIIα protein complexes were purified from DSP-treated FLAG-dysbindin (Figure 1C) or FLAG-muted–expressing cells (Figure 1D). FLAG-tagged BLOC-1 subunits dysbindin or muted specifically eluted from PI4KIIα immunoaffinity chromatography matrices with the PI4KIIα peptide 51–70 but not by buffer alone (Figure 1, C and D; compare lanes 3′ and 5′). Outcompetition with a molar excess of PI4KIIα peptide during the incubation of cell extracts with PI4KIIα antibody matrices abrogated the association of PI4KIIα and associated proteins such as endogenous BLOC-1 subunits (Figure 1, C and D, compare lanes 3 and 4) as well as FLAG-tagged dysbindin and muted (Figure 1C–D; compare lanes 4′ and 5′). Conversely, FLAG immunoaffinity chromatography from FLAG-muted–expressing cell extracts isolated PI4KIIα (Figure 1E, lanes 7 and 8). The specificity of these associations was determined by performing FLAG immunoaffinity chromatography from untransfected SH-SY5Y cells (Figure 1E, lanes 5 and 6). These data indicate that dysbindin forms complexes with AP-3 and the membrane protein cargo PI4KIIα, in addition to dysbindin's inclusion into the BLOC-1 complex.

Dysbindin's interactions with other BLOC-1 components, as well as with AP-3, and PI4KIIα, suggest that these proteins act together on a common trafficking pathway. We tested this hypothesis genetically by determining whether PI4KIIα phenotypes observed in dysbindin-null *sandy* brain (*Dtnbp1*$^{sdy/sdy}$) were phenocopied in other BLOC-1–deficient mice *muted* (*Muted*$^{mu/mu}$) and *pallid* (*Pldn*$^{pa/pa}$) and the AP-3–deficient allele *mocha* (*Ap3d1*$^{mh/mh}$; Kantheti *et al.*, 1998; Huang *et al.*, 1999; Zhang *et al.*, 2002; Li *et al.*, 2003). We analyzed PI4KIIα by quantitative confocal immunofluorescence microscopy of the dentate gyrus in the hippocampal formation (Figure 2). The dentate gyrus is where we previously observed a strong decrease in the levels of the AP-3 cargo VAMP7 in BLOC-1–deficient *muted* and *pallid* mice (Newell-Litwa *et al.*, 2010). PI4KIIα content was decreased in the neuropil of dysbindin-null *sandy* dentate gyrus (Figure 2, A and E). This phenotype was similar in BLOC-1–null mice, either by deficiency of muted or pallidin (Figure 2, B, C, and E), and the AP-3–deficient *mocha* allele (Figure 2, D and F). The selectivity of this PI4KIIα phenotype is highlighted by the absence of an effect on synaptophysin, a membrane protein targeted to synaptic vesicles by mechanisms independent of AP-3 or BLOC-1 (Salazar *et al.*, 2004b, 2006; Newell-Litwa *et al.*, 2009, 2010). The biochemical interactions among the BLOC-1 complex, AP-3, and PI4KIIα as well as the common hippocampal PI4KIIα phenotypes in BLOC-1 and AP-3 deficiencies, demonstrate that these components belong to common trafficking pathway in neuronal tissue.

PI4KIIα is depleted in nerve terminals of mice deficient in the AP-3 complex

The subcellular compartment affected by reduced levels of PI4KIIα in the mutant mice carrying deficiencies in either BLOC-1 or AP-3 was identified by subcellular fractionation and quantitative immuno–electron microscopy of brain tissue. We focused on AP-3–null brains to facilitate these experiments because AP-3–null brain phenotypes are widespread, in contrast to BLOC-1 deficiency phenotypes, which are predominantly observed in the dentate gyrus of the hippocampus (Kantheti *et al.*, 1998; Newell-Litwa *et al.*, 2010). High-speed pellets (P2) from whole-brain homogenates were sedimented in Percoll density gradients to resolve fractions enriched in pinched-off nerve terminals or heavy synaptosomes (Figure 3, HS). Levels of SV2 and synaptophysin—two synaptic vesicle markers—remained unaffected in AP-3 *mocha* (*Ap3d1*$^{mh/mh}$)-heavy synaptosomes. In contrast, the content of PI4KIIα and the synaptic vesicle AP-3 cargoes VAMP7 and ZnT3 were reduced in *Ap3d1*$^{mh/mh}$-heavy synaptosomes. ZnT3 reduction in synaptosomes was due to decreased ZnT3 levels in *Ap3d1*$^{mh/mh}$ homogenates. In contrast, PI4KIIα was significantly diminished in synaptosomes of *Ap3d1*$^{mh/mh}$ brains without changes in total homogenate levels (Figure 3). This pattern is similar to that of VAMP7 (Figure 3), a membrane protein present in synaptic vesicles that we and others demonstrated to be decreased in nerve terminals of AP-3–null brains (Scheuber *et al.*, 2006; Newell-Litwa *et al.*, 2010).

We further explored the subcellular localization of PI4KIIα in the hippocampal formation of wild-type and *Ap3d1*$^{mh/mh}$ mice by immunocytochemistry with a PI4KIIα-specific antibody (Figure 4 and Supplemental Figures S1 and S2). At the light-microscopic level, PI4KIIα displayed a distinctive distribution in different regions of the

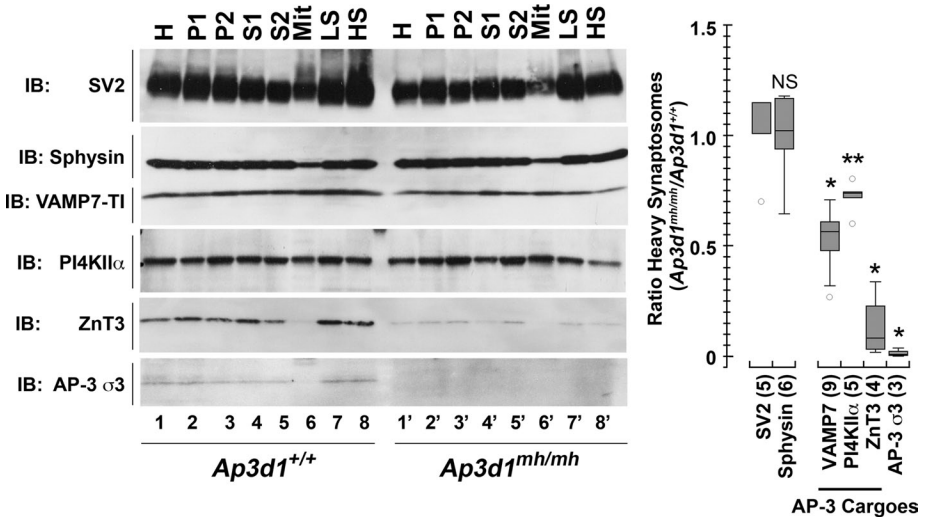

FIGURE 3: PI4KIIα content in synaptosomes of AP-3–deficient *mocha* mice is reduced. (A) Synaptosome fractions from control brains (lanes 1–8) and AP-3–deficient *mocha* (*Ap3d1*$^{mh/mh}$) brains (lanes 1′–8′) were resolved on SDS–PAGE, and the contents were analyzed by immunoblot with antibodies against synaptic vesicle markers (SV2, synaptophysin), AP-3–dependent synaptic vesicle cargoes (PI4KIIα, VAMP7, ZnT3), and AP-3 σ3 subunit. (B) Quantification of antigen content expressed as a ratio of the heavy synaptosome fraction from control and AP-3–deficient *mocha* (*Ap3d1*$^{mh/mh}$) brains. Numbers in parentheses represent the number of independent immunoblots performed from three independent fractionations. *p < 0.0001; **p = 0.0157. HS, heavy synaptosomes; LS, light synaptosomes; Mit, mitochondrial-enriched fractions obtained from Percoll gradients; P1 and P2, low- and high-speed pellets, respectively. Fractions were generated as per Nagy and Delgado-Escueta (1984).

hippocampal formation. Immunoreactivity was most prominent in cell bodies and dendrites of hippocampal pyramidal cells and in three presynaptic fields: 1) the inner molecular layer of the dentate gyrus, which is the terminal field of axons from large neurons in the dentate hilus, 2) the dentate hilus, and 3) the stratum lucidum of CA3, which (along with the dentate hilus) is the terminal field of dentate granule cells (Supplemental Figure S2). PI4KIIα subsynaptic distribution was determined by immuno–electron microscopy of the dentate gyrus. Immunoreactivity was present in dendrites (data not shown) and presynaptic elements of asymmetric axodendritic and axospinous synapses (Figure 4, A, A1, and C). PI4KIIα immunoreactivity in presynaptic elements is consistent with previous reports of PI4KIIα localization on synaptic vesicles (Guo *et al.*, 2003; Salazar *et al.*, 2005; Takamori *et al.*, 2006). We quantified the number of PI4KIIα-positive synaptic elements in the dentate gyrus hilus of wild-type and mutant mice (Figure 4, C–E). Most PI4KIIα-labeled elements were asymmetric axospinous terminals in the mouse dentate gyrus hilus (Figure 4C). Three-fourths of those nerve terminals were PI4KIIα immunoreactive in wild-type mice (*Ap3d1*$^{+/+}$). In contrast, only 35% of such terminals were PI4KIIα positive in AP-3–null *Ap3d1*$^{mh/mh}$ (Figure 4D). Because AP-3 deficiency did not affect the density of asymmetric axospinous terminals in the dentate (Figure 4E), the reduction in the density of such terminals positive for PI4KIIα reflects depletion of the enzyme in them.

Disruption of AP-3, BLOC-1, and PI4KIIα interactions impairs PI4KIIα targeting from cell body to processes

PI4KIIα depletion in nerve terminals might reflect failed export of this cargo from the parent cell bodies. We addressed this by expressing enhanced green fluorescent protein (EGFP)–tagged PI4KIIα or a dileucine-sorting mutant version of PI4KIIα that is unable to bind AP-3 or coprecipitate with the BLOC-1 complex, PI4KIIαL60-61A (Craige *et al.*, 2008; Salazar *et al.*, 2009). PI4KIIα is targeted to brain synaptic vesicles and PC12 cell synaptic-like microvesicles by AP-3 and BLOC-1 mechanisms (Salazar *et al.*, 2005; Newell-Litwa *et al.*, 2009). Moreover, synaptic-like microvesicles are coated with AP-3 and BLOC-1 complexes (Salazar *et al.*, 2005, 2006). Thus we determined the targeting of tagged PI4KIIα to PC12 synaptic-like microvesicles isolated by sucrose velocity sedimentation (Lichtenstein *et al.*, 1998). Endosomes and synaptic-like microvesicles sediment in fractions 5–7 and 15 in these gradients, respectively (Clift-O'Grady *et al.*, 1998; Lichtenstein *et al.*, 1998). Wild-type EGFP-PI4KIIα was present in endosome and synaptic-like microvesicle fractions isolated from PC12 cells (Supplemental Figure S3). In contrast, EGFP-PI4KIIαL60-61A targeting to synaptic-like microvesicle fractions was reduced (Supplemental Figure S3, A and B) concomitantly with an increased EGFP-PI4KIIαL60-61A content in endosomes (Supplemental Figure S3B; compare open and closed circles). We then used nerve growth factor (NGF)–differentiated PC12 cells and assessed EGFP-PI4KIIα distribution by imaging live and fixed specimens (Figure 5). Wild-type PI4KIIα was enriched at neurite tips of differentiated PC12 cells (Figure 5, A and A1). In contrast, the EGFP-PI4KIIαL60-61A mutant signal was faint in neurites and their tips (Figure 5, C and C1). We depicted these dramatic differences in subcellular localization as *x*, *y* coordinates, where each dot depicts an individual cell defined by its PI4KIIα fluorescence intensity in cell bodies (*x*-axis) and processes (*y*-axis; Figure 5, E and F). Decomposition of these *x*, *y*–coordinate plots into cell body and process PI4KIIα fluorescence intensities (Figure 5, G and H) revealed that cells expressed similar cell body levels per voxel of wild-type or mutant EGFP-PI4KIIα (Figure 5G). However, they differed significantly in the amount of PI4KIIα present in cell processes and their tips (Figure 5H). Similar results were obtained with fixed differentiated PC12 cells, where the EGFP-PI4KIIαL60-61A mutant levels in processes were selectively reduced compared with VAMP2, a synaptic vesicle marker whose targeting is not affected by AP-3 or BLOC-1 deficiencies (Figure 5I; Salazar *et al.*, 2004a; Newell-Litwa *et al.*, 2009).

Next we performed fluorescence recovery after photobleaching (FRAP) of PC12 cell neurite tips expressing recombinant PI4KIIα to determine 1) whether EGFP-PI4KIIα is delivered in an anterograde manner and 2) whether the EGFP-PI4KIIα delivery mechanism could be distinguished from EGFP-PI4KIIαL60-61A, as predicted by the reduced targeting of this mutant to synaptic-like microvesicles (Supplemental Figure S3). EGFP-PI4KIIα FRAP of the neurite tip reached a plateau by 45 min (Figure 6, A and B). In contrast, the EGFP-PI4KIIαL60-61A mutant recovery was accelerated, attaining steady state by 10 min (Figure 6, A and B). Rapid fluorescence recovery of PI4KIIαL60-61A could be due to diffusion of a plasma membrane EGFP-PI4KIIαL60-61A pool. This hypothesis stems from the observation that AP-3 cargoes are misrouted to the cell surface when the cargo–adaptor association is perturbed (Dell'Angelica *et al.*, 1999; Peden *et al.*, 2004). To address this, we compared EGFP-PI4KIIαL60-61A FRAP to an EGFP targeted to the plasma membrane by the palmitoylation signal of GAP43

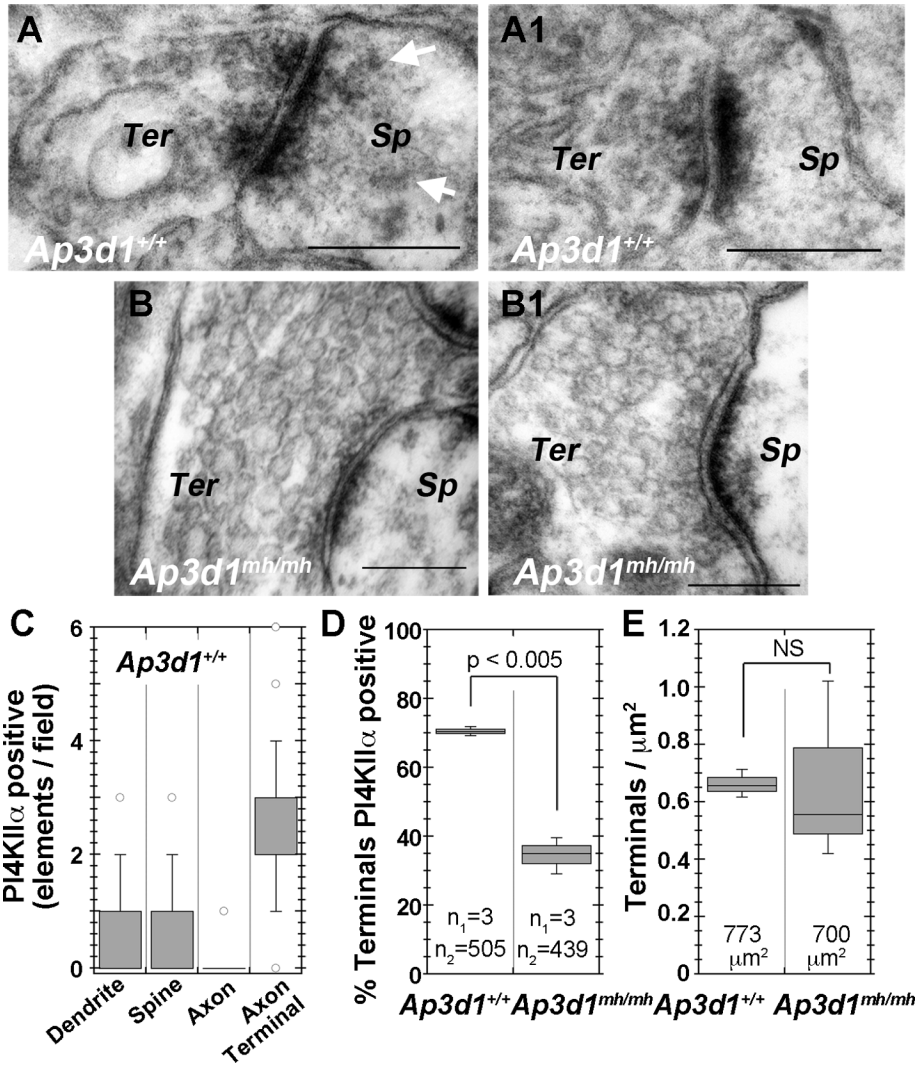

FIGURE 4: PI4KIIα is present in synapses, and its presynaptic levels are decreased in AP-3–null brains (*Ap3d1*$^{mh/mh}$). (A, A1) PI4KIIα immunoperoxidase labeling in the active zone of axon terminals forming asymmetric, axospinous synapses in the dentate gyrus of a wild-type mouse (*Ap3d1*$^{+/+}$). (B, B1) The lack of such labeling in a AP-3–null *mocha* mouse (*Ap3d1*$^{mh/mh}$). Note that the spine in A also displays a low level of immunoreactivity (arrows). (C) Relative prevalence of neural elements immunoreactive for PI4KIIα in random fields of view of the dentate gyrus taken at a magnification of 75,000× in three wild-type animals. One hundred thirty-four dentate gyrus fields were analyzed from three mice. (D) Percentage of PI4KIIα-positive terminals over the total number of asymmetric synapses counted in control and AP-3–null *mocha* (*Ap3d1*$^{mh/mh}$) dentate gyrus sections. Here, n1 corresponds to number of animals, and n2 is the number of terminals scored per genotype. Note the significant difference in percentage of labeled terminals between wild-type and AP-3–null *mocha* mice. (F) Total number of axon terminals forming axospinous, asymmetric synapses per square micron of dentate gyrus tissue in three control and three AP-3–null *mocha* (*Ap3d1*$^{mh/mh}$) mice. Numbers in the boxplot are the total area of tissue analyzed. Scale bars, 200 nm.

(EGFP-GAP43-ps), since PI4KIIα is anchored to membranes by palmitate (Figure 6, A and C; Matsuda and Cepko, 2007; Barylko *et al.*, 2009). EGFP-PI4KIIαL60-61A and EGFP-GAP43-ps FRAP were similar, suggesting that EGFP-PI4KIIαL60-61A rapid recovery is due to plasma membrane diffusion. These results indicate that wild-type PI4KIIα uses a vesicular delivery mechanism to neurite tips that is high capacity and low speed. However, a PI4KIIα mutant unable to bind AP-3 reaches PC12 neurite tips by a low-capacity mechanism compatible with diffusion in the plane of the membrane.

These experiments indicated that impairment of an AP-3, BLOC-1, and PI4KIIα interaction prevents cargo inclusion into synaptic-like microvesicles and thereby prevents PI4KIIα delivery to neurite tips in PC12 cells either assessed in vivo or in fixed specimens. To complement the results obtained with PC12 cells, we analyzed primary cultured neurons to determine whether PI4KIIα targeting to neurites was sensitive to the ablation of AP-3, the dileucine-sorting motif in PI4KIIα, and/or BLOC-1. We analyzed the distribution of PI4KIIα and the synaptic vesicle protein VAMP2 in 7-d in vitro cultures of cortical neurons (7 DIV). Fluorescence intensity in cell bodies and processes was scored for PI4KIIα and VAMP2, and values were represented as *x*, *y* coordinates (Figures 7 and 8). In wild-type neurons, endogenous PI4KIIα and VAMP2 were present in cell bodies and neuronal processes, but in *Ap3d1*$^{mh/mh}$ neurons the content of PI4KIIα in cell bodies and processes was selectively reduced (Figure 7A, B, and E1). VAMP2 distribution was not affected in this AP-3 deficiency (Figure 7, A, B, and E2). We also expressed EGFP-PI4KIIα in wild-type and AP-3–null *mocha* cells (Figure 7, C, D, and F). Targeting of EGFP-PI4KIIα to processes was impaired in *Ap3d1*$^{mh/mh}$ neurons despite cell body expression levels of EGFP-PI4KIIα spanning one order of magnitude (compare Figure 7, E1 and F1). Processes of wild-type neurons were efficiently populated by EGFP-PI4KIIα in that range of cell body expression levels (Figure 7F1). As in neurons lacking AP-3, those expressing mutant PI4KIIα unable to bind AP-3 and coprecipitate with BLOC-1 (EGFP-PI4KIIαL60-61A; Craige *et al.*, 2008; Salazar *et al.*, 2009) failed to populate cell processes (Figure 7, G1–H1). This EGFP-PI4KIIαL60-61A phenotype was observed irrespective of the culture age and recombinant protein expression level in cell bodies (Figure 7, G1–H1). The selectivity of these phenotypes was demonstrated by unaltered VAMP2 distribution (Figure 7, G2–H2). Our data demonstrate that integrity of interaction between the AP-3 adaptor and its cargo, PI4KIIα, is required for cargo export from cell bodies to neurites.

PI4KIIα association to AP-3 requires BLOC-1, and deficiencies in BLOC-1 complex subunits phenocopied a PI4KIIα phenotype in the AP-3–null dentate gyrus (Figure 2). Thus we tested whether endogenous PI4KIIα, EGFP-PI4KIIα, and EGFP-PI4KIIαL60-61A export from cell bodies to neurites was impaired in dysbindin-BLOC-1–deficient *sandy Dtnbp1*$^{sdy/sdy}$ neurons (Figure 8). We focused on dysbindin-null neurons because of strong association of dysbindin gene polymorphisms with schizophrenia (Ross *et al.*, 2006; Allen *et al.*, 2008; Sun *et al.*, 2008; Talbot *et al.*, 2009). Control (*Dtnbp1*$^{+/+}$) and dysbindin-BLOC-1–null neurons (*Dtnbp1*$^{sdy/sdy}$) expressed either

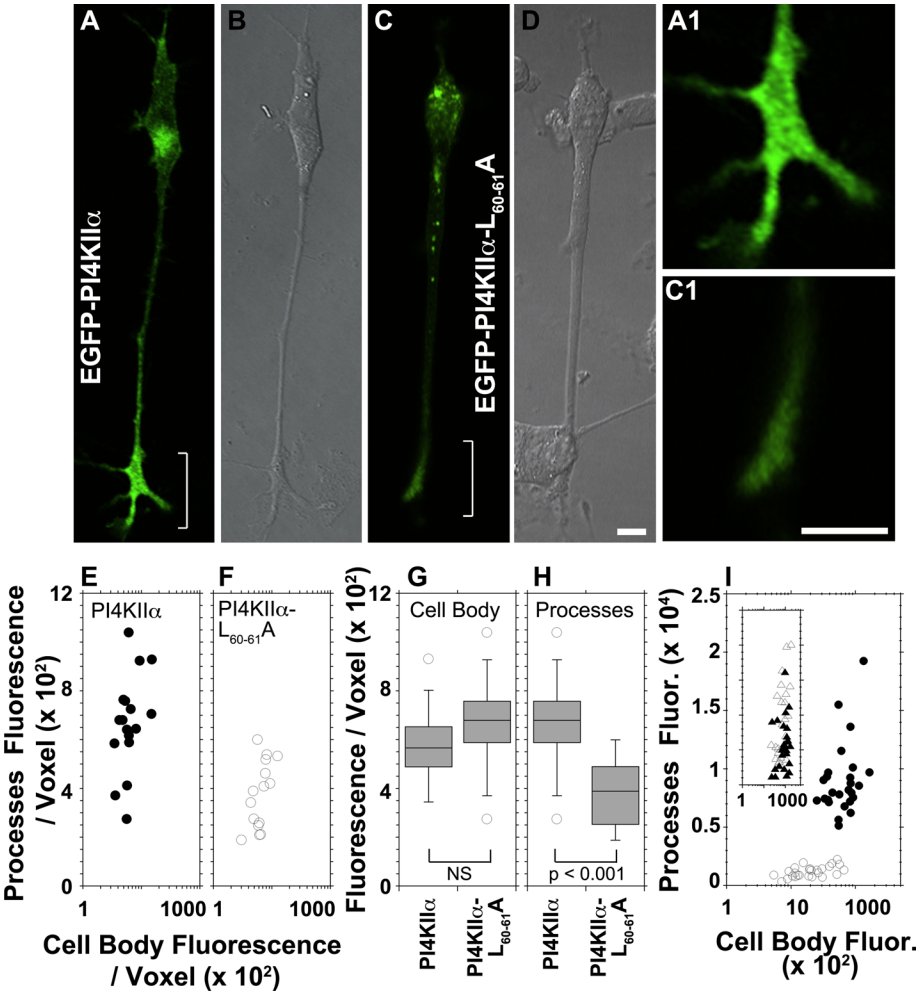

FIGURE 5: PI4KIIα targeting to neurites in PC12 cells requires the PI4KIIα dileucine-sorting motif. PC12 cells expressing wild-type EGFP-PI4KIIα (A, B; n = 17 cells) or EGFP-PI4KIIαL60-61A (C, D; n = 15 cells) tagged with EGFP were NGF differentiated for 48–72 h posttransfection and cells were imaged in vivo. (B, D) DIC images. (A1, C1) Enlarged view of neurite tips in A and C. (E, F) Fluorescence intensity per voxel was measured for wild-type PI4KIIα-expressing (closed circles) and PI4KIIαL60-61A-expressing (open circles) cells both in cell bodies and their processes. (H,G) Comparison of fluorescence intensity between PI4KIIα- and PI4KIIαL60-61A–expressing cells from E and F for cell bodies and processes, respectively. (I) Transfected cells were stained for VAMP2 and EGFP and imaged by confocal fluorescence microscopy. Fluorescent pixels present in cell body and processes were quantified for both VAMP2 and transfected PI4KIIα. Closed symbols depict data from cells expressing wild-type PI4KIIα (n = 26 cells), whereas open symbols depict fluorescent pixels from cells expressing PI4KIIαL60-61A (n = 26). Circles and triangles represent EGFP and VAMP2 fluorescence values, respectively. In E, F, and I, each point depicts the fluorescence intensity in processes and cell body of individual cells as in terms of *x*, *y* coordinates. Data were collected from three independent experiments. Bars, 10 μm.

endogenous (Figure 8E) or EGFP-PI4KIIα to a similar extent in cell bodies (Figure 8, A, C, and F). However, PI4KIIα or EGFP-PI4KIIα did not populate neurites in *Dtnbp1*$^{sdy/sdy}$ neurons (Figure 8, E and F; compare closed circles [*Dtnbp1*$^{+/+}$] and open circles [*Dtnbp1*$^{sdy/sdy}$]). EGFP-PI4KIIαL60-61A remained constrained to cell bodies both in control and BLOC-1–null *sandy* cells (Figure 8G). All PI4KIIα phenotypes were selective, since the distribution of VAMP2 in neurons was not affected by the *Dtnbp1*$^{sdy/sdy}$ allele or the expression of wild-type or mutant forms of PI4KIIα (Figure 8, E1–F1; compare closed triangles [*Dtnbp1*$^{+/+}$] and open triangles [*Dtnbp1*$^{sdy/sdy}$]). Therefore, the dysbindin-containing BLOC-1 complex is required for the delivery of PI4KIIα to neurites from neuronal perikarya.

DISCUSSION

We showed here that the schizophrenia susceptibility gene product dysbindin, which is contained in the BLOC-1 complex, and its interacting AP-3 adaptor are required to target cargoes into vesicles assembled at cell bodies for delivery into neurites and nerve terminals. These carriers selectively deliver a subset of synaptic vesicle membrane proteins to the synapse. In contrast, synaptic vesicle proteins such as synaptophysin and VAMP2 are not affected by null alleles of these protein complexes. We explored the BLOC-1–AP-3 transport mechanism by assessing the subcellular distribution and movement of PI4KIIα, a lipid kinase that both binds to AP-3 by a BLOC-1–dependent mechanism and regulates AP-3 recruitment to endosomes (Craige *et al.*, 2008; Salazar *et al.*, 2009). PI4KIIα is depleted in dentate gyrus neuropil of dysbindin-null *sandy* mice, a trait phenocopied in mice deficient in the dysbindin-interacting BLOC-1 subunits muted and pallidin and in AP-3–null mice carrying the *Ap3d1*$^{mh/mh}$ *mocha* allele. The common PI4KIIα phenotype among these four mutant mice results from disrupted association of PI4KIIα with BLOC-1 and AP-3. PI4KIIα was retained in the cell body of neurons lacking AP-3 or BLOC-1 protein complexes, a phenotype emulated by mutagenesis of the dileucine-sorting motif in PI4KIIα. This motif is necessary for PI4KIIα association with AP-3, its copurification with BLOC-1, and its exit from early endosomes in human fibroblastoid cells (Craige *et al.*, 2008; Salazar *et al.*, 2009).

We predicted the existence of a BLOC-1–AP-3 pathway that delivers vesicles from cell bodies to nerve terminals from our "seesaw" sorting hypothesis (Newell-Litwa *et al.*, 2009). This seesaw model was postulated to explain the opposing effects that ubiquitous and neuronal AP-3–null alleles had in cargo delivery to synaptic vesicle fractions (Newell-Litwa *et al.*, 2009). A BLOC-1–AP-3 route between cell bodies and nerve terminals was further supported by the existence of 1) BLOC-1– and AP-3–decorated vesicle carrier in PC12 cells (Salazar *et al.*, 2005 2006), 2) the presence of a BLOC-1–AP-3 supracomplex in isolated nerve terminals (synaptosomes; Newell-Litwa *et al.*, 2010), and 3) BLOC-1– and AP-3–null nerve terminal phenotypes in brain tissue in toto (Newell-Litwa *et al.*, 2010). However, points 1–3 were similarly compatible with a local role of BLOC-1 and AP-3 in nerve terminals. Moreover, such a local role is additionally supported by the observation that AP-3–dependent mechanisms acutely regulate vesicle traffic in nerve terminals (Voglmaier *et al.*, 2006). Thus the origin of BLOC-1 and AP-3 vesicles in neurons remained an untested prediction from our previous work. Our data presented here demonstrate that the cell body is the most upstream site where BLOC-1 and AP-3 are required for membrane protein sorting toward the synapse. This

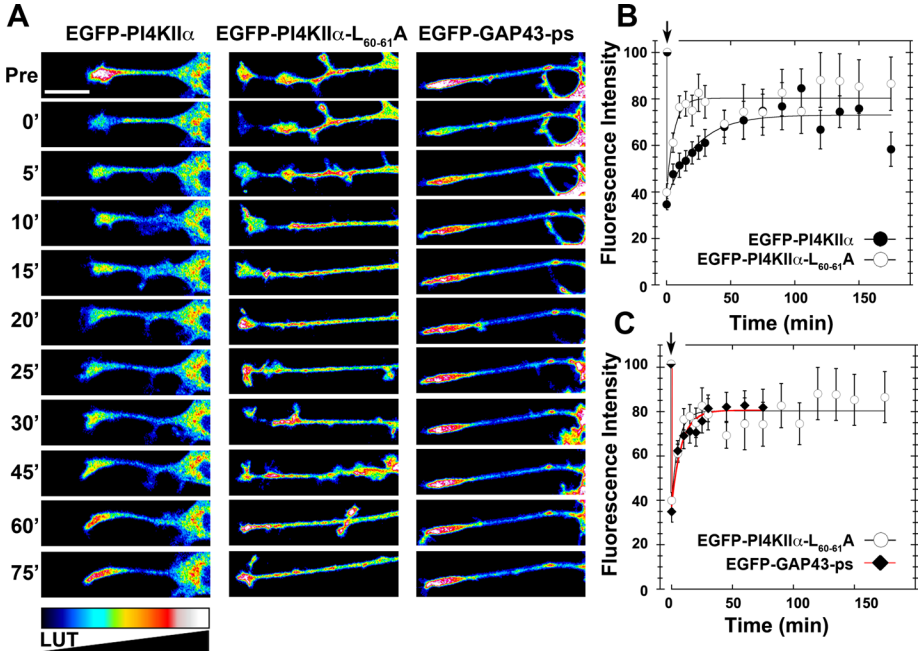

FIGURE 6: Distinct mechanisms mediate the delivery of wild-type and dileucine mutant PI4KIIα into neurites. (A) Look-up table (LUT) of photobleached neurite tips of PC12 cells expressing EGFP-PI4Kα, EGFP-PI4KIIαL60-61A, or EGP-GAP43-ps. In vivo images were taken before (Pre), during photobleaching (0') and every 5 min thereafter for 30 min, after which an image was acquired every 15 min for an additional 45 min. (B, C) Time course of neurite tip fluorescence intensity (%) during FRAP, normalized to their fluorescence intensity before photobleaching. (B) EGFP-PI4KIIαL60-61A (n = 14 cells) recovers faster than EGFP-PI4Kα (n = 23 cells) following photobleaching, reaching a plateau within 10 min vs. 45 min, respectively. (C) No differences are observed in the time course of recovery between EGFP-PI4KIIαL60-61A and EGP-GAP43-ps (n = 8 cells). Scale bars, 20 μm.

is clearly illustrated by the trapping of endogenous and exogenously expressed PI4KIIα in cell bodies of neurons defective in either BLOC-1 or AP-3. In addition to the assembly and loading of vesicular carriers in the cell body, it is possible that BLOC-1 and AP-3 may perform functions along axons and dendrites, because subunits of these complexes are found in these subcellular compartments (Zakharenko *et al.*, 1999; Talbot *et al.*, 2006; Newell-Litwa *et al.*, 2010). Although our data clearly indicate that BLOC-1 and AP-3 function in a common vesicular transport pathway, especially in the transport of the PI4KIIα cargo, it is also possible that BLOC-1 complexes may generate vesicles independent of AP-3. This possibility is supported by the observation that ATP7A targeting to melanosomes requires only BLOC-1 (Setty *et al.*, 2008).

It is likely that PI4KIIα is just one of the proteins trafficked from cell bodies to neurites via the pathway identified here. We predict that other vesicular cargoes are also affected in BLOC-1 and AP-3 deficiencies. The soluble *N*-ethylmaleimide–sensitive factor attachment protein receptor (SNARE) protein VAMP7, also known as TI-VAMP, is a probable candidate for trafficking with PI4KIIα in vesicles assembled by BLOC-1–AP-3 (Salazar *et al.*, 2006; Scheuber *et al.*, 2006; Newell-Litwa *et al.*, 2010). VAMP7 is present in a subset of nerve terminals in the brain, which in the hippocampal formation (Muzerelle *et al.*, 2003) are distributed in a manner very similar to that described here for PI4KIIα. Moreover, VAMP7 is reduced in the dentate gyrus of AP-3–null *mocha* mice and BLOC-1–null *muted* mice (Scheuber *et al.*, 2006; Newell-Litwa *et al.*, 2010). The spectrum of vesicles and their cargoes may also include those targeted to dendritic compartments. Dendritic carriers assembled by BLOC-1 and/or AP-3 could deliver membrane cargoes bound to dendritic compartments from cell bodies. This hypothesis is supported by the presence of PI4KIIα in both cell bodies and dendritic compartments as demonstrated here, as well as AP-3 and dysbindin as demonstrated previously (Talbot *et al.*, 2004, 2006, 2011; Seong *et al.*, 2005; Newell-Litwa *et al.*, 2010). Alternatively, BLOC-1 and/or AP-3 could participate in the local recycling of specific membrane proteins, such as the dopamine D2 receptor and the NR2A subunit of the *N*-methyl-D-aspartic acid receptor, to and from the synaptic plasma membrane (Iizuka *et al.*, 2007; Ji *et al.*, 2009; Tang *et al.*, 2009b; Marley and von Zastrow, 2010). Impaired cargo delivery not only could affect membrane dynamics in mature neurons but also could impair the development of neuronal processes (Ghiani *et al.*, 2009; Ito *et al.*, 2010).

Presynaptic or postsynaptic functional deficits in neurons lacking either BLOC-1 or AP-3 complexes likely result from the type of proteins depleted from synapses and the extent of their depletion. For example, vesicle fusion may be impaired as a result of reduced PI4KIIα and SNAREs, including VAMP7. Consistent with this, dysbindin *sandy* mice and a knockout of the BLOC-1 subunit snapin reveal a role for BLOC-1 complex subunits in modulating calcium-regulated exocytosis of chromaffin granules and synaptic vesicles (Ilardi *et al.*, 1999; Tian *et al.*, 2005; Chen *et al.*, 2008; Pan *et al.*, 2009). Similarly, *Drosophila* dysbindin functions presynaptically in adaptive homeostatic modulation of vesicle release (Dickman and Davis, 2009). Of importance, these changes in the physiology of presynaptic secretory organelles occur concomitant with changes in organelle morphology. Chromaffin granules from dysbindin-null mice are larger, a phenotype observed in both chromaffin granules and synaptic vesicles from dentate gyrus glutamatergic terminals of the AP-3 *mocha* mouse (Grabner *et al.*, 2006; Chen *et al.*, 2008; Newell-Litwa *et al.*, 2010). These similar morphological changes in dysbindin and AP-3–null cells further support that BLOC-1 and AP-3 participate in the same pathway.

Dysbindin, its interacting partner pallidin (unpublished data), and AP-3 are widely expressed in the brain. Judging from the synaptic fields in which dysbindin is concentrated and the synaptic effects of dysbindin loss (Talbot *et al.*, 2004, 2006, 2009; Iizuka *et al.*, 2007; Chen *et al.*, 2008; Ji *et al.*, 2009; Tang *et al.*, 2009b; Papaleo *et al.*, 2010), multiple neurotransmitter systems (especially dopamine, GABA, and glutamate) may be affected by deficiencies in the dysbindin/BLOC-1/AP-3 pathway. Because vesicle-trafficking mechanisms control the subcellular delivery of multiple membrane proteins to nerve terminals, defects in specific membrane-protein sorting events are almost certainly involved in the diverse neurochemical phenotypes observed in schizophrenia, given widespread synaptic dysbindin reductions observed in the disorder (Talbot *et al.*, 2004, 2011; Tang *et al.*, 2009a). We propose that pathways defined by schizophrenia susceptibility genes, such as the dysbindin/BLOC-1/AP-3 pathway, offer encompassing mechanisms to explain multiple, pleiotropic neurochemical and neurodevelopmental phenotypes observed in schizophrenia brains.

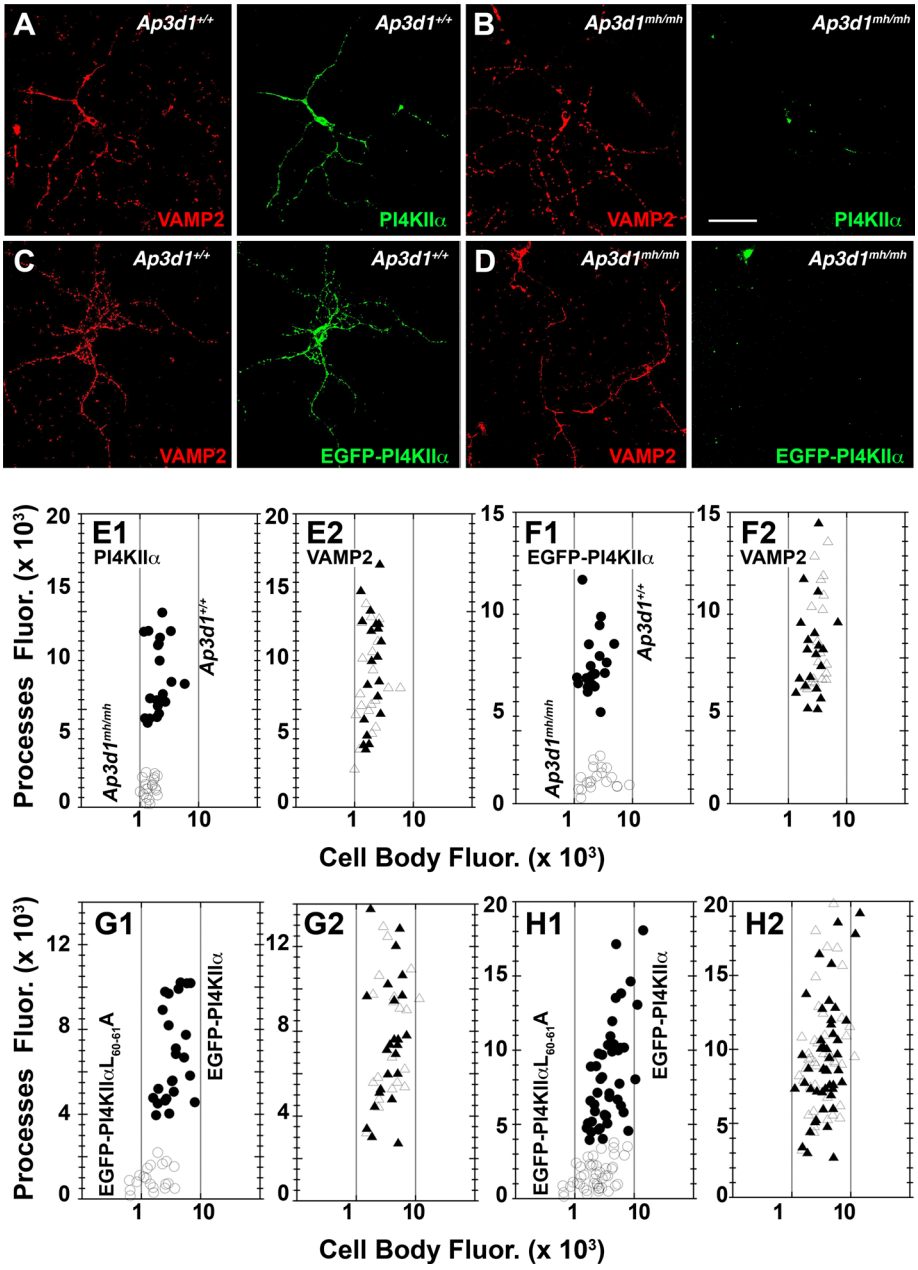

FIGURE 7: PI4KIIα targeting to neuronal processes is impaired in AP-3–deficient *mocha* (*Ap3d1*$^{mh/mh}$) neurons. Primary cultured forebrain P4 neurons from wild-type (*Ap3d1*$^{+/+}$) (A, C) or AP-3–deficient *mocha* mice (*Ap3d1*$^{mh/mh}$) (B, D) either untransfected (A, B) or transfected (C, D) with EGFP-PI4KIIα were cultured for 7DIV. Cells were stained for VAMP2 (red) and either EGFP (green) or endogenous PI4KIIα (green) and imaged by confocal fluorescence microscopy. Fluorescent pixels present in the cell body and processes were quantified for both VAMP2 and either endogenous (E) or transfected PI4KIIα (F) and presented as cell body–to–processes fluorescence intensity *x*, *y* coordinates. Closed symbols depict data from wild-type neurons, whereas open symbols depict fluorescent pixels from AP-3–null *mocha* neurons. Circles and triangles represent PI4KIIα and VAMP2 fluorescence values, respectively. Each point represents an individual neuron. (G, H) Primary cultured forebrain P4 neurons from wild-type mice expressing PI4KIIα or PI4KIIαL60-61A tagged with EGFP were cultured for either 7DIV (H) or 3DIV (G). Cells were stained for VAMP2 and EGFP and imaged by confocal fluorescence microscopy. Fluorescent pixels present in cell body and processes were quantified for both VAMP2 and transfected PI4KIIα (G, H). Closed symbols depict data from cells expressing wild-type PI4KIIα, whereas open symbols depict fluorescent pixels from cells expressing PI4KIIαL60-61A. Circles and triangles represent EGFP and VAMP2 fluorescence values, respectively. E1, E2, n = 20 cells; F1, F2, n = 20 wild-type and AP-3–null cells (*Ap3d1*$^{mh/mh}$); G1, G2, n = 24 EGFP-PI4KIIα–transfected cells and n = 20 EGFP-PI4KIIαL60-61A–transfected cells; H1, H2, n = 49 EGFP-PI4KIIα–transfected and n = 45 EGFP-PI4KIIαL60-61A–transfected cells. All neurons were obtained from three independent experiments. Scale bars, 50 μm.

MATERIALS AND METHODS

Antibodies, plasmids, recombinant proteins, and mice

The following antibodies were used in this study: mouse monoclonals against AP3-δ (SA4) and SV2 from the Developmental Studies Hybridoma Bank at the University of Iowa (Iowa City, IA), synaptophysin (SY38) from Chemicon International/Millipore (Billerica, MA), and VAMP7-TI (a generous gift of Andrew Peden, Cambridge University, Cambridge, United Kingdom), as well as rabbit polyclonals against PI4KIIα peptide 51-71 PGHDRERQPLLDRARGAAAQ (Uniprot/Swiss-Prot entry Q99M64 [P4K2A_RAT] UniProtKB/Swiss-Prot) generated in this study and VAMP-2 from Synaptic Systems (Göttingen, Germany). Chicken anti-GFP was obtained from Aves Labs (Tigard, OR). Rat monoclonal anti-HA was from Roche (Indianapolis, IN). Glutathione *S*-transferase full fusion protein of PI4KIIα was prepared as previously described (Craige *et al.*, 2008). pEGFP-C2 wild-type rat PI4KIIα and pEGFP-C2-PI4KIIαL60-61A mutant plasmids were previously described (Craige *et al.*, 2008). C-Terminally FLAG-tagged muted (EXT4795-M14) and N-terminal–tagged FLAG-tagged Dysbindin (EX-Mm12550-M12) were obtained from Genecopoeia (Rockville, MD). Both constructs were in a pReceiver vector backbone, and sequences were independently confirmed. EGFP-GAP43-ps was expressed from pCAG-mGFP Addgene (Cambridge, MA) plasmid 14757 (Matsuda and Cepko, 2007).

mocha (STOCK gr +/+ Ap3d1^{mh}/J, here referred to as *Ap3d1*$^{mh/mh}$) and its control *grizzled* (STOCK gr +/+ Ap3d1^{+}/J, here referred to as *Ap3d*$^{+/+}$) and *pallid* (B6.Cg-Pldn^{pa}/J, here referred to as *Pldn*$^{pa/pa}$) breeding mouse pairs were obtained from Jackson Labs (Bar Harbor, ME) and bred in-house following Institutional Animal Care and Use Committee (IUCAC)–approved protocols. Muted mice and their controls (B6C3 *A*$^{w\text{-}J}$/*A-Muted*^{mu}/J, *Muted*$^{mu/mu}$, and CHMU$^{+/mu}$; Zhang *et al.*, 2002) were obtained from Richard Swank (Roswell Park Cancer Institute, Buffalo, NY) and bred in-house. *Sandy* mice in C57B6 background were previously described (Cox *et al.*, 2009). All mice were bred in-house following IUCAC-approved protocols.

Cell culture

Cerebrocortical neurons were cultured from postnatal day 4 (P4) mice (*Ap3d1*$^{+/+}$, *Ap3*$^{mh/mh}$, *CHMU*, *muted*, *C57* and *sandy*) and maintained in neurobasal media containing B27, L-glutamine, and 100 μg/ml penicillin and streptomycin (Hyclone, Logan,

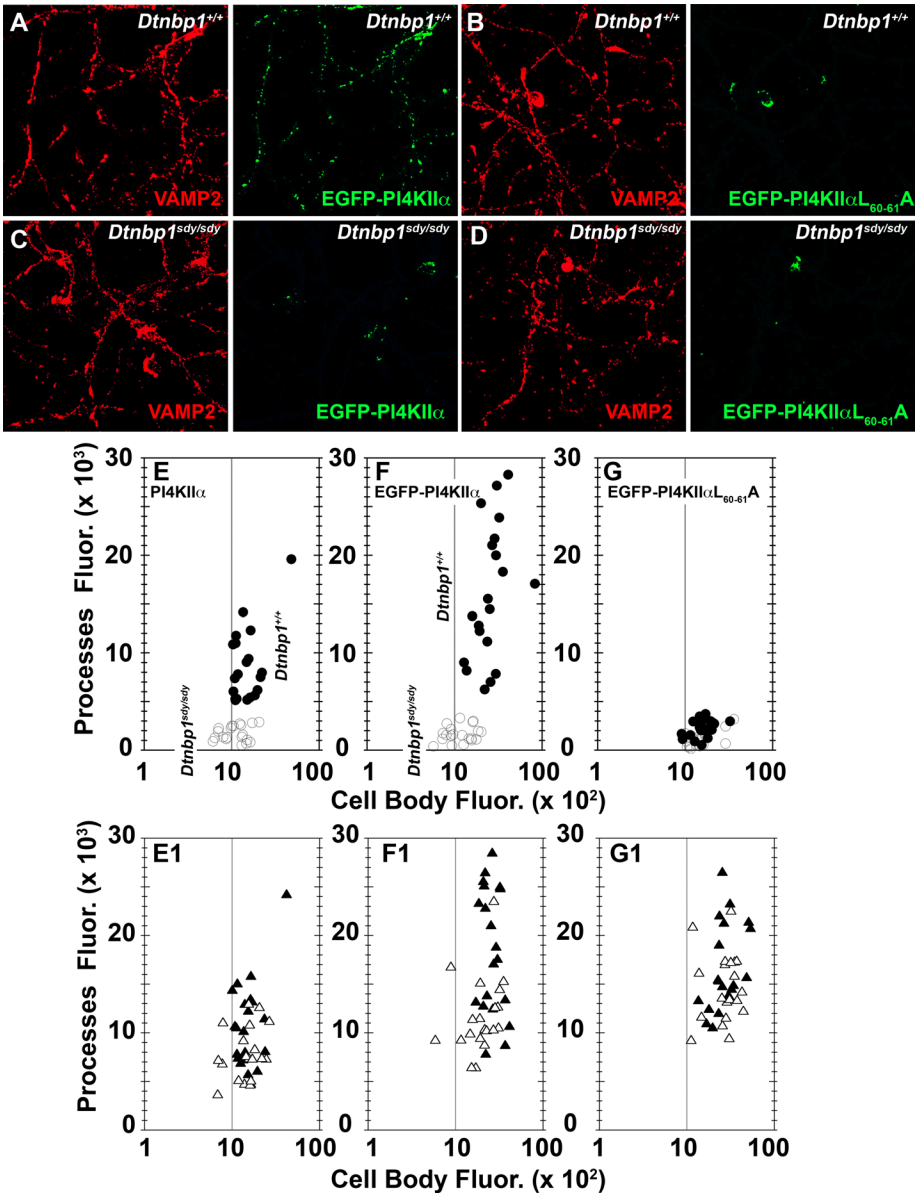

FIGURE 8: PI4KIIα targeting to neuronal processes is impaired in BLOC-1–deficient neurons. Primary cultured forebrain neurons from control (*Dtnbp1*$^{+/+}$) (A, B) or dysbindin-BLOC-1–deficient *sandy* mice (*Dtnbp1*$^{sdy/sdy}$ (C, D) either not transfected (E) or transfected with EGFP-PI4KIIα (A, C) or EGFP-PI4KIIαL60-61A (B, D) were cultured for 7DIV. Cells were stained for VAMP2 (red) and PI4KIIα for untransfected cells or VAMP2 and EGFP (green) for transfected cells. Fixed cells were imaged by confocal fluorescence microscopy. Fluorescent pixels present in cell body and processes were quantified for VAMP2 (E1, F1, G1), endogenous PI4KIIα (E), and transfected PI4KIIα (F, G) cells. Closed circles depict PI4KIIα or EGFP fluorescent pixels from wild-type neurons, whereas open circles depict pixels from dysbindin-BLOC-1–null *sandy* neurons. Closed triangles depict VAMP2 fluorescent pixels from wild-type neurons, whereas open triangles depict pixels from dysbindin-BLOC-1–null *sandy* neurons. Each point represents an individual neuron. Twenty neurons per condition were obtained from three independent experiments. Scale bars, 50 μm.

UT) at 5% CO_2 and 37°C. Dissociated neurons were plated on poly-L-lysine (Sigma-Aldrich, St. Louis, MO)–coated glass coverslips and cultured for 3–7 d in vitro (DIV). Dissociated neurons (2×10^6) were transfected with 3 μg of plasmid DNA using Amaxa nucleofection electroporation (Lonza, Cologne, Germany). Neurons were plated at a density of 6×10^4 cells per well in a 12-well plate.

HEK-293, SH-SY5Y, wild-type and pallidin-deficient mouse skin primary culture fibroblasts, and PC12 cells (American Type Culture Collection, Manassas, VA) were cultured in DMEM supplemented with either 10% fetal bovine serum (FBS) or, in the case of PC12 cells, a mix of 5% FBS plus 10% equine serum, respectively (Hyclone). Media were supplemented with 100 μg/ml penicillin and streptomycin (Hyclone). Cells were maintained at 37°C with 10% CO_2. PC12 cells were transfected with 3 μg/μl DNA by nucleofection using Amaxa Cell Line Nucleofector Kit V (Lonza) and plated in PC12 culture media supplemented with 100 ng/ml NGF 2.5S (murine, natural) (Invitrogen, Carlsbad, CA) on Matrigel-coated, glass-bottom culture dishes (MaTek, Ashland, MA). PC12 cells were differentiated for 48–72 h at 37°C with 10% CO_2.

Immunohistochemistry

We analyzed PI4KIIα distribution using two immunoperoxidase-labeling protocols. First, 11 male and 11 female C57BL6/J mice 3–6 mo old were deeply anesthetized with sodium pentobarbital (1.0 mg/kg) and perfused transcardially with saline, followed by neutral buffered Formalin. Their brains were then postfixed in the same fixative overnight, embedded in paraffin, and sectioned coronally at 6 μm. The sections were mounted and air dried. They were next dewaxed in xylenes, rehydrated in descending concentrations of ethanol, and immersed for 30 min in 5% hydrogen peroxide dissolved in absolute methanol to quench endogenous peroxidase activity. Following a 10-min water rinse, the tissue was subjected to antigen retrieval by boiling in 1 mM EDTA in 0.1 M Tris buffer, pH 8.0, for 10 min (Pileri *et al.*, 1997). After cooling and rinsing, the sections were reacted immunohistochemically with the PI4KIIα antibody (1:300) generated for this study using a standard avidin/biotin/peroxidase method with nickel sulfate amplification of the 3,3′-diaminobenzidine (DAB) reaction product (Talbot *et al.*, 2004). Results were analyzed on a BX61 Olympus (Center Valley, PA) research microscope equipped with an Olympus DP71 cooled charge coupled device (CCD) digital camera.

Immuno–electron microscopy

Tissue used in brain slice preparations was obtained from either male or female mice between 6 and 8 wk of age, unless otherwise indicated. Following deep anesthesia with Nembutal, animals were transcardially perfused with fixative (4% paraformaldehyde with 0.1% glutaraldehyde). Brains were postfixed in 4% paraformaldehyde, which was replaced with phosphate-buffered saline (PBS) within 12–18 h. With use of a vibrating microtome, brains were cut into 60-μm-thick sections and stored in antifreeze (0.1 M sodium phosphate monobasic, 0.1 M sodium phosphate

dibasic heptahydrate, 30% ethylene glycol, 30% glycerol) at −20°C until immunohistochemical preparation.

The 60-μm-thick brain sections were rinsed in PBS and then incubated in sodium borohydride, followed by 100% cryoprotectant (phosphate buffer 0.05 M, pH 7.4, 25% sucrose, 10% glycerol) for 20 min at −80°C and returned to decreasing amounts of cryoprotectant. Sections were preincubated in PBS with 1% normal horse serum (NHS) and 1% BSA, followed by primary antibody incubation with 1:500 affinity-purified anti-PI4KIIα. Sections were rinsed in PBS and then incubated in a secondary goat anti–rabbit immunoglobulin G antibody solution (1:1000 dilution) (Jackson ImmunoResearch Labs, West Grove, PA) for 90 min at room temperature. Sections were rinsed with PBS and then incubated in a 1:1000 dilution of rabbit peroxidase antiperoxidase (Jackson ImmunoResearch Labs). Sections were rinsed in PBS with a final rinse in Tris buffer (50 mM, pH 7.6) before a 10-min incubation in 0.025% DAB, 1 mM imidazole, and 0.005% hydrogen peroxide in Tris buffer at room temperature. At this point sections were mounted and analyzed by light microcopy or they were further processed for electron microscopy after rinsing sections in phosphate buffer (0.1 M, pH 7.4). Sections were incubated in 1% osmium tetroxide for 10 min and then returned to phosphate buffer before being dehydrated in increasing concentrations of ethanol. At the 70% ethanol incubation, 1% uranyl acetate was added, and sections were incubated in the dark for 35 min. After dehydration, sections were treated with propylene oxide and embedded in epoxy resin overnight (Durcupan ACM; Fluka, Buschs, Switzerland). Next tissues were mounted onto slides and incubated at 60°C for 48 h. Tissue samples of the dentate gyrus were removed from the slides, mounted on resin blocks, cut into 60-nm-thick sections, collected on Pioloform-coated copper grids, and stained with lead citrate for 5 min.

Electron microscopy was performed with a Zeiss EM-10C electron microscope with a CCD camera (DualView 300W; Gatan, Pleasanton, CA). Images were acquired with Gatan Digital Micrograph Software, version 3.10.1 (Gatan). Analysis was focused on the interface between the granule cells and hilar neuropil, where PI4KIIα was concentrated across mice strains. In the electron microscope, only tissue areas from the surface of the blocks with optimal antibody penetration were examined. These sections were scanned at 10,000×, and random fields of view containing at least one asymmetric synapse were photographed at 75,000×. One hundred ninety micrographs from three blocks of tissue in three animals covering 773 μm^2 were examined for the control and 172 micrographs from three blocks of tissue in three animals covering 700 μm^2 were examined. From this material, the total number of PI4KIIα-immunoreactive or immunonegative terminals forming asymmetric axospinous synapses was counted to estimate the relative percentage of positively labeled terminals. In addition, in wild-type (*Ap3d1*$^{+/+}$) mice, all positive immunoperoxidase-labeled neuronal elements in the field were counted and categorized as axons, spines, dendrites, or glia, based on ultrastructural criteria defined by Peters *et al*. (1991). Light microscopy of brain sections was performed with a Leica DMRB microscope with a 10×/0.3 differential interference contrast (DIC) objective (Leica Microsystems, Bannockburn, IL), and images were captured with a CCD camera and the Leica IM50 software (Leica DC500).

Immunofluorescence labeling for confocal microscopy

Confocal microscopy was performed with an Axiovert 100M microscope (Carl Zeiss, Jena, Germany) coupled to Ar and He–Ne lasers. Images were acquired using Plan Apochromat 10×/0.5 dry, 20×/0.5 dry, and 40×/1.3 and 63×/1.4 DIC oil objectives. Emission filters used for fluorescence imaging were BP 505-530 and LP 560. Images were acquired with ZEN and LSM 510 software (Carl Zeiss). Hippocampal-formation 60-μm-thick brain sections were first rinsed with PBS and then incubated in 1% sodium borohydride in PBS for 20 min at room temperature, followed by extensive washing with PBS. Samples were preincubated in a solution of PBS with 5% NHS and 1% BSA and 0.3% Triton X-100 for 60 min at room temperature. Samples were incubated overnight at 4°C in primary antibody solutions of PBS with 1% NHS and 1% BSA and anti-PI4KIIα with anti-synaptophysin (SY38) (dilutions of 1:500 and 1:10,000, respectively). After rinsing in PBS, sections were incubated for 60 min in a secondary antibody PBS solution with 1% NHS and 1% BSA and 1:500 dilutions of the following Alexa-conjugated secondary antibodies: anti–mouse 555 (for anti-synaptophysin) and anti–rabbit 488 (for anti-PI4KIIα) (Invitrogen Molecular Probes, Carlsbad, CA). Following PBS rinses, sections were incubated in cupric sulfate (3.854 wt/vol ammonium acetate, 1.596 wt/vol cupric sulfate in distilled water, pH 5) for 30 min. Sections were washed with PBS and mounted on slides with Vectashield (Vector Laboratories, Burlingame, CA).

HEK293 cells, PC12 cells, and cortical neurons were washed in ice-cold PBS and fixed in 4% paraformaldehyde for 20 min on ice. Cells were then incubated in blocking solution (2% BSA plus 1% fish skin gelatin plus 15% horse serum plus 0.02% saponin in PBS) for 30 min at room temperature. Next cells were incubated with antibody for 30 min at 37°C, rinsed, and then incubated with secondary antibody diluted in block for 30 min at 37°C. Cells were then rinsed and mounted with Gelvatol and sealed. Cortical neurons were selected from a field of neurons using the following criteria. Neurons were chosen where a single neuron could be discerned from neighboring neurons, where the morphology met the criteria for the proper development in vitro (Goslin and Banker, 1989), and only chosen based on the staining of the control vesicle marker illuminating the entire neuron. Micrographs were analyzed by creating a region of interest (ROI) outlining only the axon or only the cell body and then determining total number of fluorescent pixels in that specific ROI for the VAMP2 channel and the PI4KIIα channel.

Live imaging of PC12 cells expressing PI4KIIα-GFP, PI4KIIαL60-61A-GFP, or EGFP-GAP43-ps was performed on an A1R Laser Scanning Confocal Microscope (Nikon, Melville, NY) equipped with a hybrid scanner, Perfect Focus, and an environmental chamber for regulation of temperature to 37°C and 10% CO_2. Confocal images with a Z-step of 1μm were captured for 10 min (no delay) with an Apo total internal reflection fluorescence 60×/1.49 oil differential interference contrast (DIC) objective on NIS-Elements AR 3.1 (Nikon) software. Neurite tips of PC12 cells were photobleached for 2 s at 30% laser power. Images were captured for 15 s (no delay) before photobleaching and for 15 min every 5 min after photobleaching, followed by 2 h every 15 min. PC12 cell imaging was performed in Hank's balanced salt solution minus phenol red and $NaHCO_2$ (Sigma-Aldrich) and supplemented with 10% Donor Equine Serum (Hyclone), 5% fetal bovine serum (Hyclone), and 100 ng/ml NGF 2.5S. Imaris 6.3.1 (Bitplane, St. Paul, MN) and ImageJ 1.41 (National Institutes of Health, Bethesda, MD) software were used for image analysis. For FRAP experiments an ROI representing neurite tips was selected, and fluorescence intensity was measured using ImageJ and normalized to a second ROI in the cell body to compensate for photobleaching due to imaging. Voxel fluorescence intensity was measured in neurites and cell bodies of PC12 cells using Imaris software.

Synaptosome preparation

Synaptosomes were prepared according to Nagy and Delgado-Escueta (1984) from 4-wk-old mice. Briefly, mice were anesthetized by CO_2 and brains quickly transferred to ice cold PBS. Tissue was homogenized by 16 strokes of a Potter-Elvehjem homogenizer at 800 rpm in 0.32 M sucrose, 5 mM 4-(2-hydroxyethyl)-1-piperazineethanesulfonic acid (HEPES), and 0.5 mM EDTA supplemented with Complete antiprotease inhibitor (Roche). Homogenates were spun at 1000 × *g* for 10 min, and S1 supernatants were further sedimented at 12,000 × *g* for 20 min. This P2 pellet was resuspended in 8.5% Percoll (Sigma-Aldrich) and then loaded on a discontinuous gradient comprised of 10 and 16% Percoll. Gradients were spun at 15,000 × *g* for 20 min.

Microvesicle isolation

PC12 cell microvesicles were prepared as described (Clift-O'Grady *et al.*, 1998). Briefly, cells were lifted from culture dishes with PBS plus 5 mM EDTA on ice. Cells were spun at 800 rpm for 5 min and resuspended in bud buffer (38 mM potassium aspartate, 38 mM potassium glutamate, 38 mM potassium gluconate, 20 mM 4-morpholinepropanesulfonic acid, pH 7.2, 5 mM reduced glutathione, 5 mM sodium carbonate, 2.5 mM magnesium sulfate) and spun again for 5 min at 800 rpm. Cells were then passed through the cell homogenizer (Isobiotec, Heidelberg, Germany) for 16 passes. Cell homogenates were spun for 5 min at 1000 × *g* and supernatant resolved 10–45% sucrose gradient. Gradient were spun in a SW55 rotor for 1 h at 116,000 × *g* (Lichtenstein *et al.*, 1998).

Immunoaffinity chromatography

To assess low-affinity interactions between PI4KIIα, AP-3, and BLOC-1 subunits, we performed cross-linking in intact cells with DSP (Craige *et al.*, 2008; Salazar *et al.*, 2009; Zlatic *et al.*, 2010). Briefly, SHSY5Y cells stably transfected either with FLAG-dysbindin or FLAG-muted were placed on ice, rinsed twice with PBS, and incubated either with 10 mM DSP (Pierce, Rockford, IL) or as a vehicle control DMSO, diluted in PBS for 2 h on ice. Tris, pH 7.4, was added to the cells for 15 min to quench the DSP reaction. The cells were then rinsed twice with PBS and lysed in buffer A (150 mM NaCl, 10 mM HEPES, 1 mM ethylene glycol tetraacetic acid, and 0.1 mM $MgCl_2$, pH 7.4) with 0.5% Triton X-100 by incubation for 30 min on ice. Cells were scraped from the dish, and cell homogenates were centrifuged at 16,100 × *g* for 10 min. The clarified supernatant was recovered, and at least 500 µg was applied to 30 µl of Dynal magnetic beads (Invitrogen) coated with antibody and incubated for 2 h at 4°C. In some cases, immunoprecipitations were done in the presence of the antigenic peptide as a control. The beads were then washed four to six times with buffer A with 0.1% Triton X-100. Proteins were eluted from the beads either with sample buffer or by 2 h of incubation with 200 µM antigenic peptide (either PI4KIIα peptide 51-71 or 3× FLAG peptide) on ice. Samples were resolved by SDS–PAGE and contents analyzed by immunoblot.

Statistical analysis

Experimental conditions were compared with the nonparametric Wilcoxon–Mann–Whitney rank sum test or one-way analysis of variance, Dunnett's multiple comparison using Synergy KaleidaGraph, version 4.03 (Reading, PA) or StatPlus Mac Built5.6.0pre/Universal (AnalystSoft, Vancouver, Canada). Data are presented as boxplots displaying the four quartiles of the data, with the "box" comprising the two middle quartiles, separated by the median. The upper and lower quartiles are represented by the single lines extending from the box.

ACKNOWLEDGMENTS

This work was supported by grants from the National Institutes of Health to V.F. (NS42599, GM077569). We are indebted to the Faundez lab members for their comments. This work was supported in part by Neuronal Imaging Core of the Emory Neuroscience National Institute for Neurological Disorders and Stroke Core Facilities Grant P30NS055077.

REFERENCES

Allen NC, Bagade S, McQueen MB, Ioannidis JP, Kavvoura FK, Khoury MJ, Tanzi RE, Bertram L (2008). Systematic meta-analyses and field synopsis of genetic association studies in schizophrenia: the SzGene database. Nat Genet 40, 827–834.

Barylko B, Mao YS, Wlodarski P, Jung G, Binns DD, Sun HQ, Yin HL, Albanesi JP (2009). Palmitoylation controls the catalytic activity and subcellular distribution of phosphatidylinositol 4-kinase IIalpha. J Biol Chem 284, 9994–10003.

Bhardwaj SK, Baharnoori M, Sharif-Askari B, Kamath A, Williams S, Srivastava LK (2009). Behavioral characterization of dysbindin-1 deficient sandy mice. Behav Brain Res 197, 435–441.

Bonifacino JS, Glick BS (2004). The mechanisms of vesicle budding and fusion. Cell 116, 153–166.

Borck G *et al.* (2008). Clinical, cellular, and neuropathological consequences of AP1S2 mutations: further delineation of a recognizable X-linked mental retardation syndrome. Hum Mutat 29, 966–974.

Burgos PV, Mardones GA, Rojas AL, daSilva LL, Prabhu Y, Hurley JH, Bonifacino JS (2010). Sorting of the Alzheimer's disease amyloid precursor protein mediated by the AP-4 complex. Dev Cell 18, 425–436.

Cheli VT *et al.* (2010). Genetic modifiers of abnormal organelle biogenesis in a *Drosophila* model of BLOC-1 deficiency. Hum Mol Genet 19, 861–878.

Chen XW *et al.* (2008). DTNBP1, a schizophrenia susceptibility gene, affects kinetics of transmitter release. J Cell Biol 181, 791–801.

Clift-O'Grady L, Desnos C, Lichtenstein Y, Faundez V, Horng JT, Kelly RB (1998). Reconstitution of synaptic vesicle biogenesis from PC12 cell membranes. Methods 16, 150–159.

Cox MM, Tucker AM, Tang J, Talbot K, Richer DC, Yeh L, Arnold SE (2009). Neurobehavioral abnormalities in the dysbindin-1 mutant, sandy, on a C57BL/6J genetic background. Genes Brain Behav 8, 390–397.

Craige B, Salazar G, Faundez V (2008). Phosphatidylinositol-4-kinase type II alpha contains an AP-3 sorting motif and a kinase domain that are both required for endosome traffic. Mol Biol Cell 19, 1415–1426.

Deborde S, Perret E, Gravotta D, Deora A, Salvarezza S, Schreiner R, Rodriguez-Boulan E (2008). Clathrin is a key regulator of basolateral polarity. Nature 452, 719–723.

Dell'Angelica EC (2009). AP-3-dependent trafficking and disease: the first decade. Curr Opin Cell Biol 21, 552–559.

Dell'Angelica EC, Shotelersuk V, Aguilar RC, Gahl WA, Bonifacino JS (1999). Altered trafficking of lysosomal proteins in Hermansky-Pudlak syndrome due to mutations in the beta 3A subunit of the AP-3 adaptor. Mol Cell 3, 11–21.

Di Pietro SM, Dell'Angelica EC (2005). The cell biology of Hermansky-Pudlak syndrome: recent advances. Traffic 6, 525–533.

Di Pietro SM, Falcon-Perez JM, Tenza D, Setty SR, Marks MS, Raposo G, Dell'Angelica EC (2006). BLOC-1 interacts with BLOC-2 and the AP-3 complex to facilitate protein trafficking on endosomes. Mol Biol Cell 17, 4027–4038.

Dickman DK, Davis GW (2009). The schizophrenia susceptibility gene dysbindin controls synaptic homeostasis. Science 326, 1127–1130.

Dwyer ND, Adler CE, Crump JG, L'Etoile ND, Bargmann CI (2001). Polarized dendritic transport and the AP-1 mu1 clathrin adaptor UNC-101 localize odorant receptors to olfactory cilia. Neuron 31, 277–287.

Folsch H, Ohno H, Bonifacino JS, Mellman I (1999). A novel clathrin adaptor complex mediates basolateral targeting in polarized epithelial cells. Cell 99, 189–198.

Folsch H, Pypaert M, Maday S, Pelletier L, Mellman I (2003). The AP-1A and AP-1B clathrin adaptor complexes define biochemically and functionally distinct membrane domains. J Cell Biol 163, 351–362.

Ghiani CA, Dell'Angelica EC (2011). Dysbindin-containing complexes and their proposed functions in brain: from zero to (too) many in a decade. ASN Neuro 3, e00058.

Ghiani CA, Starcevic M, Rodriguez-Fernandez IA, Nazarian R, Cheli VT, Chan LN, Malvar JS, de Vellis J, Sabatti C, Dell'Angelica EC (2009). The dysbindin-containing complex (BLOC-1) in brain: developmental

regulation, interaction with SNARE proteins and role in neurite outgrowth. Mol Psychiatry 15, 204–215.
Glyvuk N, Tsytsyura Y, Geumann C, D'Hooge R, Huve J, Kratzke M, Baltes J, Boening D, Klingauf J, Schu P (2010). AP-1/sigma1B-adaptin mediates endosomal synaptic vesicle recycling, learning and memory. EMBO J 29, 1318–1330.
Goslin K, Banker G (1989). Experimental observations on the development of polarity by hippocampal neurons in culture. J Cell Biol 108,1507–1516.
Grabner CP, Price SD, Lysakowski A, Cahill AL, Fox AP (2006). Regulation of large dense-core vesicle volume and neurotransmitter content mediated by adaptor protein 3. Proc Natl Acad Sci USA 103, 10035–10040.
Guo J, Wenk MR, Pellegrini L, Onofri F, Benfenati F, De Camilli P (2003). Phosphatidylinositol 4-kinase type IIalpha is responsible for the phosphatidylinositol 4-kinase activity associated with synaptic vesicles. Proc Natl Acad Sci USA 100, 3995–4000.
Hattori S, Murotani T, Matsuzaki S, Ishizuka T, Kumamoto N, Takeda M, Tohyama M, Yamatodani A, Kunugi H, Hashimoto R (2008). Behavioral abnormalities and dopamine reductions in sdy mutant mice with a deletion in Dtnbp1, a susceptibility gene for schizophrenia. Biochem Biophys Res Commun 373, 298–302.
Haucke V, Neher E, Sigrist SJ (2011). Protein scaffolds in the coupling of synaptic exocytosis and endocytosis. Nat Rev Neurosci 12, 127–138.
Horikawa HP, Kneussel M, El Far O, Betz H (2002). Interaction of synaptophysin with the AP-1 adaptor protein gamma-adaptin. Mol Cell Neurosci 21, 454–462.
Huang L, Kuo YM, Gitschier J (1999). The pallid gene encodes a novel, syntaxin 13-interacting protein involved in platelet storage pool deficiency. Nat Genet 23, 329–332.
Iizuka Y, Sei Y, Weinberger DR, Straub RE (2007). Evidence that the BLOC-1 protein dysbindin modulates dopamine D2 receptor internalization and signaling but not D1 internalization. J Neurosci 27, 12390–12395.
Ilardi JM, Mochida S, Sheng ZH (1999). Snapin: a SNARE-associated protein implicated in synaptic transmission. Nat Neurosci 2, 119–124.
Ito H, Morishita R, Shinoda T, Iwamoto I, Sudo K, Okamoto K, Nagata K (2010). Dysbindin-1, WAVE2 and Abi-1 form a complex that regulates dendritic spine formation. Mol Psychiatry 15, 976–986.
Ji Y, Yang F, Papaleo F, Wang HX, Gao WJ, Weinberger DR, Lu B (2009). Role of dysbindin in dopamine receptor trafficking and cortical GABA function. Proc Natl Acad Sci USA 106, 19593–19598.
Kantheti P *et al.* (1998). Mutation in AP-3 delta in the mocha mouse links endosomal transport to storage deficiency in platelets, melanosomes, and synaptic vesicles. Neuron 21, 111–122.
Karayiorgou M, Simon TJ, Gogos JA (2010). 22q11.2 microdeletions: linking DNA structural variation to brain dysfunction and schizophrenia. Nat Rev Neurosci 11, 402–416.
Lasiecka ZM, Winckler B (2011). Mechanisms of polarized membrane trafficking in neurons— focusing in on endosomes. Mol Cell Neurosci 48, 278–287.
Li W, Rusiniak ME, Chintala S, Gautam R, Novak EK, Swank RT (2004). Murine Hermansky-Pudlak syndrome genes: regulators of lysosome-related organelles. Bioessays 26, 616–628.
Li W *et al.* (2003). Hermansky-Pudlak syndrome type 7 (HPS-7) results from mutant dysbindin, a member of the biogenesis of lysosome-related organelles complex 1 (BLOC-1). Nat Genet 35, 84–89.
Lichtenstein Y, Desnos C, Faundez V, Kelly RB, Clift-O'Grady L (1998). Vesiculation and sorting from PC12-derived endosomes in vitro. Proc Natl Acad Sci USA 95, 11223–11228.
Lomant AJ, Fairbanks G (1976). Chemical probes of extended biological structures: synthesis and properties of the cleavable protein cross-linking reagent [35S]dithiobis(succinimidyl propionate). J Mol Biol 104, 243–261.
Marley A, von Zastrow M (2010). Dysbindin promotes the post-endocytic sorting of G protein-coupled receptors to lysosomes. PLoS ONE 5, e9325.
Matsuda S, Miura E, Matsuda K, Kakegawa W, Kohda K, Watanabe M, Yuzaki M (2008). Accumulation of AMPA receptors in autophagosomes in neuronal axons lacking adaptor protein AP-4. Neuron 57, 730–745.
Matsuda S, Yuzaki M (2009). Polarized sorting of AMPA receptors to the somatodendritic domain is regulated by adaptor protein AP-4. Neurosci Res 65, 1–5.
Matsuda T, Cepko CL (2007). Controlled expression of transgenes introduced by in vivo electroporation. Proc Natl Acad Sci USA 104, 1027–1032.
Montpetit A *et al.* (2008). Disruption of AP1S1, causing a novel neurocutaneous syndrome, perturbs development of the skin and spinal cord. PLoS Genet 4, e1000296.
Moreno-De-Luca A, Helmers SL, Mao H, Burns TG, Melton AM, Schmidt KR, Fernhoff PM, Ledbetter DH, Martin CL (2011). Adaptor protein complex-4 (AP-4) deficiency causes a novel autosomal recessive cerebral palsy syndrome with microcephaly and intellectual disability. J Med Genet 48, 141–144.
Mullin AP, Gokhale A, Larimore J, Faundez V (2011). Cell biology of the BLOC-1 complex subunit dysbindin, a schizophrenia susceptibility gene. Mol Neurobiol 44, 53–64.
Muzerelle A, Alberts P, Martinez-Arca S, Jeannequin O, Lafaye P, Mazie JC, Galli T, Gaspar P (2003). Tetanus neurotoxin-insensitive vesicle-associated membrane protein localizes to a presynaptic membrane compartment in selected terminal subsets of the rat brain. Neuroscience 122, 59–75.
Nagy A, Delgado-Escueta AV (1984). Rapid preparation of synaptosomes from mammalian brain using nontoxic isoosmotic gradient material (Percoll). J Neurochem 43, 1114–1123.
Newell-Litwa K, Chintala S, Jenkins S, Pare JF, McGaha L, Smith Y, Faundez V (2010). Hermansky-Pudlak protein complexes, AP-3 and BLOC-1, differentially regulate presynaptic composition in the striatum and hippocampus. J Neurosci 30, 820–831.
Newell-Litwa K, Salazar G, Smith Y, Faundez V (2009). Roles of BLOC-1 and AP-3 complexes in cargo sorting to synaptic vesicles. Mol Biol Cell 20, 1441–1453.
Pan PY, Tian JH, Sheng ZH (2009). Snapin facilitates the synchronization of synaptic vesicle fusion. Neuron 61, 412–424.
Papaleo F, Yang F, Garcia S, Chen J, Lu B, Crawley JN, Weinberger DR (2010). Dysbindin-1 modulates prefrontal cortical activity and schizophrenia-like behaviors via dopamine/D2 pathways. Mol Psychiatry. doi:10.1038/mp.2010.106 [Epub ahead of print].
Peden AA, Oorschot V, Hesser BA, Austin CD, Scheller RH, Klumperman J (2004). Localization of the AP-3 adaptor complex defines a novel endosomal exit site for lysosomal membrane proteins. J Cell Biol 164, 1065–1076.
Peters A, Palay SL, Webster H (1991). Fine Structure of the Nervous System: Neurons and Their Supporting Cells, New York: Oxford University Press.
Pileri SA *et al.* (1997). Antigen retrieval techniques in immunohistochemistry: comparison of different methods. J Pathol 183, 116–123.
Raposo G, Marks MS (2007). Melanosomes—dark organelles enlighten endosomal membrane transport. Nat Rev Mol Cell Biol 8, 786–797.
Robinson MS (2004). Adaptable adaptors for coated vesicles. Trends Cell Biol 14, 167–174.
Ross CA, Margolis RL, Reading SA, Pletnikov M, Coyle JT (2006). Neurobiology of schizophrenia. Neuron 52, 139–153.
Ryder PV, Faundez V (2009). Schizophrenia: the "BLOC" may be in the endosomes. Sci Signal 2, pe66.
Saillour Y *et al.* (2007). Mutations in the AP1S2 gene encoding the sigma 2 subunit of the adaptor protein 1 complex are associated with syndromic X-linked mental retardation with hydrocephalus and calcifications in basal ganglia. J Med Genet 44, 739–744.
Salazar G *et al.* (2006). BLOC-1 complex deficiency alters the targeting of adaptor protein complex-3 cargoes. Mol Biol Cell 17, 4014–4026.
Salazar G, Craige B, Wainer BH, Guo J, De Camilli P, Faundez V (2005). Phosphatidylinositol-4-kinase type II alpha is a component of adaptor protein-3-derived vesicles. Mol Biol Cell 16, 3692–3704.
Salazar G, Love R, Styers ML, Werner E, Peden A, Rodriguez S, Gearing M, Wainer BH, Faundez V (2004a). AP-3-dependent mechanisms control the targeting of a chloride channel (ClC-3) in neuronal and non-neuronal cells. J Biol Chem 279, 25430–25439.
Salazar G, Love R, Werner E, Doucette MM, Cheng S, Levey A, Faundez V (2004b). The zinc transporter ZnT3 interacts with AP-3 and it is targeted to a distinct synaptic vesicle subpopulation. Mol Biol Cell 15, 575–587.
Salazar G, Zlatic S, Craige B, Peden AA, Pohl J, Faundez V (2009). Hermansky-Pudlak syndrome protein complexes associate with phosphatidylinositol 4-kinase type II alpha in neuronal and non-neuronal cells. J Biol Chem 284, 1790–1802.
Scheuber A, Rudge R, Danglot L, Raposo G, Binz T, Poncer JC, Galli T (2006). Loss of AP-3 function affects spontaneous and evoked release at hippocampal mossy fiber synapses. Proc Natl Acad Sci USA 103, 16562–16567.
Seong E, Wainer BH, Hughes ED, Saunders TL, Burmeister M, Faundez V (2005). genetic analysis of the neuronal and ubiquitous AP-3 adaptor complexes reveals divergent functions in brain. Mol Biol Cell 16, 128–140.

Setty SR, Tenza D, Sviderskaya EV, Bennett DC, Raposo G, Marks MS (2008). Cell-specific ATP7A transport sustains copper-dependent tyrosinase activity in melanosomes. Nature 454, 1142–1146.
Starcevic M, Dell'Angelica EC (2004). Identification of snapin and three novel proteins (BLOS1, BLOS2, and BLOS3/reduced pigmentation) as subunits of biogenesis of lysosome-related organelles complex-1 (BLOC-1). J Biol Chem 279, 28393–28401.
Sun J, Kuo PH, Riley BP, Kendler KS, Zhao Z (2008). Candidate genes for schizophrenia: a survey of association studies and gene ranking. Am J Med Genet B Neuropsychiatr Genet 147B, 1173–1181.
Takamori S *et al*. (2006). Molecular anatomy of a trafficking organelle. Cell 127, 831–846.
Talbot K (2009). The sandy (sdy) mouse: a dysbindin-1 mutant relevant to schizophrenia research. Prog Brain Res 179, 87–94.
Talbot K, Cho DS, Ong WY, Benson MA, Han LY, Kazi HA, Kamins J, Hahn CG, Blake DJ, Arnold SE (2006). Dysbindin-1 is a synaptic and microtubular protein that binds brain snapin. Hum Mol Genet 15, 3041–3054.
Talbot K *et al*. (2004). Dysbindin-1 is reduced in intrinsic, glutamatergic terminals of the hippocampal formation in schizophrenia. J Clin Invest 113, 1353–1363.
Talbot K, Louneva N, Cohen JW, Kazi H, Blake DJ, Arnold SE (2011). Synaptic dysbindin-1 reductions in schizophrenia occur in an isoform-specific manner indicating their subsynaptic location. PLoS ONE 6, e16886.
Talbot K, Ong WY, Blake DJ, Tang D, Louneva N, Carlson GC, Arnold SE (2009). Dysbindin-1 and its protein family, with special attention to the potential role of dysbindin-1 in neuronal functions and the pathophysiology of schizophrenia. In: Handbook of Neurochemistry and Molecular Neurobiology, Vol. 27, ed. JA Kantrowitz, New York: Springer Science, 107–241.
Tang J, LeGros RP, Louneva N, Yeh L, Cohen JW, Hahn CG, Blake DJ, Arnold SE, Talbot K (2009a). Dysbindin-1 in dorsolateral prefrontal cortex of schizophrenia cases is reduced in an isoform-specific manner unrelated to dysbindin-1 mRNA expression. Hum Mol Genet 18, 3851–3863.
Tang TT, Yang F, Chen BS, Lu Y, Ji Y, Roche KW, Lu B (2009b). Dysbindin regulates hippocampal LTP by controlling NMDA receptor surface expression. Proc Natl Acad Sci USA 106, 21395–21400.
Tarpey PS *et al*. (2006). Mutations in the gene encoding the Sigma 2 subunit of the adaptor protein 1 complex, AP1S2, cause X-linked mental retardation. Am J Hum Genet 79, 1119–1124.
Tian JH *et al*. (2005). The role of snapin in neurosecretion: snapin knock-out mice exhibit impaired calcium-dependent exocytosis of large dense-core vesicles in chromaffin cells. J Neurosci 25, 10546–10555.
Voglmaier SM, Kam K, Yang H, Fortin DL, Hua Z, Nicoll RA, Edwards RH (2006). Distinct endocytic pathways control the rate and extent of synaptic vesicle protein recycling. Neuron 51, 71–84.
Wei ML (2006). Hermansky-Pudlak syndrome: a disease of protein trafficking and organelle function. Pigment Cell Res 19, 19–42.
Winckler B, Choo Yap C (2011). Endocytosis and endosomes at the crossroads of regulating trafficking of axon outgrowth-modifying receptors. Traffic 12, 1099–1108.
Zakharenko S, Chang S, O'Donoghue M, Popov SV (1999). Neurotransmitter secretion along growing nerve processes: comparison with synaptic vesicle exocytosis. J Cell Biol 144, 507–518.
Zhang Q, Li W, Novak EK, Karim A, Mishra VS, Kingsmore SF, Roe BA, Suzuki T, Swank RT (2002). The gene for the muted (mu) mouse, a model for Hermansky-Pudlak syndrome, defines a novel protein which regulates vesicle trafficking. Hum Mol Genet 11, 697–706.
Zlatic SA, Ryder PV, Salazar G, Faundez V (2010). Isolation of labile multi-protein complexes by in vivo controlled cellular cross-linking and immuno-magnetic affinity chromatography. J Vis Exp 37, pii: 1855.